

Estimating Graph Dimension with Cross-validated Eigenvalues

Fan Chen¹, Sébastien Roch², Karl Rohe¹, and Shuqi Yu²

¹Department of Statistics, University of Wisconsin–Madison

²Department of Mathematics, University of Wisconsin–Madison

December 24, 2025

Abstract

In applied multivariate statistics, estimating the number of latent dimensions or the number of clusters, k , is a fundamental and recurring problem. We study a sequence of statistics called *cross-validated eigenvalues*. Under a large class of random graph models, including both Poisson and Bernoulli edges, without parametric assumptions, we provide a p -value for each cross-validated eigenvalue. It tests the null hypothesis that the sample eigenvector is orthogonal to (i.e., uncorrelated with) the true latent dimensions. This approach naturally adapts to problems where some dimensions are not statistically detectable. In scenarios where all k dimensions can be estimated, we show that our procedure consistently estimates k . In simulations and data example, the proposed estimator compares favorably to alternative approaches in both computational and statistical performance.

Keywords: central limit theorem, cross-validation, graph dimension, random graph

1 Introduction

In social network analysis, a large and popular class of models supposes that each person has a set of k latent characteristics and the probability that a pair of people are friends depends only on that pair’s k characteristics. Typically, for example, if two people have similar characteristics, then they are more likely to become friends. We aim to estimate the number of characteristics k using a class of models where every edge is statistically independent, conditionally on the characteristics. This includes the Latent Space Model, the Aldous-Hoover representation, and graphons [Hoff et al., 2002, Aldous, 1985, Hoover, 1989, Lovász, 2012, Jacobs and Clauset, 2014].

We are particularly interested in the class of models called the random dot product model [Athreya et al., 2013], which includes the Stochastic Blockmodel, along with its degree-corrected and mixed membership variants [Karrer and Newman, 2011, Airoldi et al., 2008]. In the Stochastic Blockmodel, k is the number of blocks.

1.1 Motivating examples

Denote the adjacency matrix $A \in \mathbb{N}^{n \times n}$ as recording the number of edges between i and j in element A_{ij} . In the models that we consider A is a random matrix and $\mathbb{E}(A)$ has k non-zero eigenvalues. We use this fact to estimate k .

The eigenvalues of A (i.e., the “sample eigenvalues”) in the scree plot unfortunately often fail to provide a clear estimate of k . As an illustration, Figure 1 shows such cases in simulated and real data. In the left panel, the simulated graph comes from a Degree-Corrected Stochastic Blockmodel, with $k = 128$ hierarchically arranged blocks. Many of the 128 dimensions cannot be estimated from the data. As such, it is not surprising that no artifacts arise in the scree plot around 128. The right panel gives the scree plot for a citation graph of 22,688 academic journals. This graph was constructed from the Semantic Scholar database [Ammar et al., 2018], where each journal is a node, and citations between two papers represent edges. In this graph, the average node degree is 35. Supplementary Section S2 provides more details on these two graphs. In Figure 1, neither panel provides clear guidance for how to choose k . This is often the fact with scree plots. Figures 2 and 3 provide an alternative plot that gives clearer guidance.

In the left panel of Figure 2, the black line is the scree plot from the left panel of Figure 1. In that same panel, the orange line gives the eigenvalues of $\mathbb{E}(A)$, i.e. the “population eigenvalues”; notice how it goes to zero at 128. In this panel, the black line is significantly greater than the orange line. This is why the standard scree plot is so difficult to use. That gap comes from *the bias of the sample eigenvalues*. This paper explains how this bias arises

We often look for an elbow or a gap in scree plots.

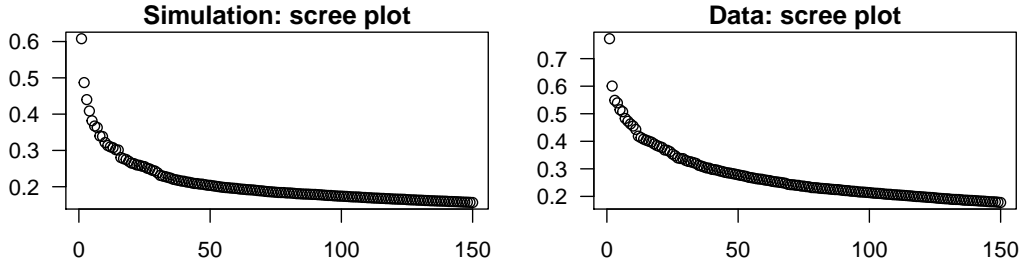


Figure 1: In these examples, it is difficult to detect a gap or elbow. In the left panel, the graph is simulated from a Degree-Corrected Stochastic Blockmodel with $n = 2560$. In the right panel, the graph is a citation graph among $n = 22,688$ academic journals. Displayed are the largest 150 eigenvalues of the normalized and regularized adjacency matrix.

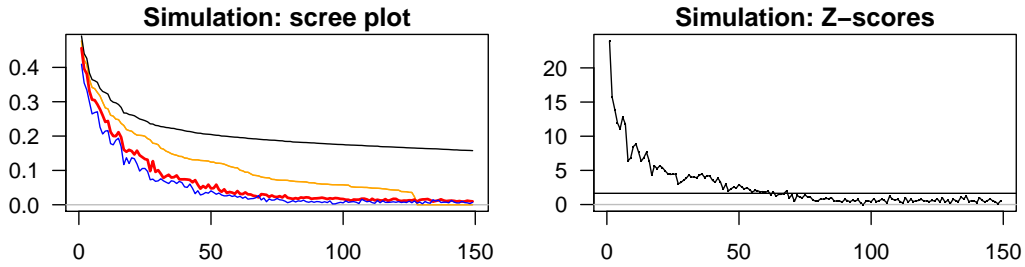


Figure 2: In the left panel, the black line gives the sample eigenvalues (repeated from the left panel of Figure 1) and the orange line gives the $k = 128$ non-zero population eigenvalues. The first two eigenvalues have been removed to improve the display. The blue line gives cross-validated eigenvalues, and the red line gives their population version, cross-population eigenvalue. In the right panel, the black line depicts the Z-scores for cross-validated eigenvalues. The horizontal black line corresponds to the cutoff for 0.05 significance level (two-side). In this example, a good choice for \hat{k} would be around 60.

from “overfitting” to the noise in the random graph.

The blue line in the left panel of Figure 2 gives our proposed *cross-validated eigenvalues*. The red line gives the population version of such quantities, named *cross-population eigenvalues*, where the $\mathbb{E}(A)$ is assumed known in place of A . The red and blue lines reveal that the signal strength of eigenvectors computed from the data diminishes after around $\hat{k} \approx 60$. Interestingly, for each cross-validated eigenvalue, one can test the null hypothesis its population counter part (the cross-population eigenvalue) is equal to zero. So, the right panel of Figure 2 gives the Z-score for each of the cross-validated eigenvalues. In that panel, the Z-scores start to cluster around the cutoff at $\hat{k} \approx 60$. The standard scree plot (black line in left panel) does not reveal anything around this value.

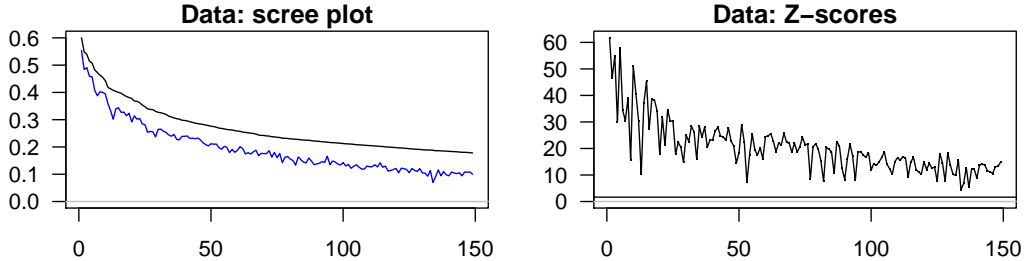


Figure 3: In the left panel, the black line gives the empirical eigenvalues (repeated from the right panel of Figure 1). The blue line gives cross-validated eigenvalues. In the right panel, the Z-scores are calculated under the null hypothesis that each cross-population eigenvalue is zero. The horizontal black line corresponds to the cutoff at 0.05 significance level.

In Figure 3, we return to the citation graph of 22,688 academic journals displayed in the right panel of Figure 1. In this example, the cross-validated eigenvalues suggest that all of the leading 150 dimensions are highly statistically significant. This is consistent with the results in Rohe and Zeng [2020] that showed the leading 100 dimensions reveal groups of journals that form coherent academic areas. It’s worth pointing out that A has 789,980 non-zero elements, spread across 22,688 rows and columns. Despite the relatively large size of this graph, computing all 150 cross-validated eigenvalues and their Z-scores requires less than 10 seconds in **R** on a 2.0GHz quad-core processor (Intel Core i5, MacBook Pro 2020). This performance is enabled by the sparse matrix packages **Matrix** and **RSpectra** [Bates and Maechler, 2021, Qiu and Mei, 2019].

1.2 Our contributions

In this paper, we exploit a notion of cross-validated eigenvalues as a new approach to estimating k . A key piece for this technique is to split the edges in the graph into two independent sets [Abbe and Sandon, 2015, Abbe et al., 2016]. Then, the eigenvectors and cross-validated eigenvalues are defined using the two graphs. This removes the bias from overfitting. Under a large class of random graph models, we provide a simple procedure to compute cross-validated eigenvalues.

A related holdout approach was previously explored in the econometrics literature [Abadir et al., 2014, Lam, 2016] for covariance estimation. In this paper and in those prior papers, the eigenvectors are estimated with a portion of the data and the “signal strength” of those vectors is estimated with the remaining held-out data. There are three key differences with this previous work. First, the observed data is of a different nature; for a covariance matrix $\Sigma \in \mathbb{R}^{p \times p}$, it is assumed in Lam [2016] that we observe $y_i = \Sigma^{1/2}x_i$,

where x_i are unobserved and contain independent, identically distributed (i.i.d.) random variables. Second, the notion of sample splitting is different; the approach in Abadir et al. [2014] constructs a sample covariance matrix with a subsample of the observed vectors y_1, \dots, y_n . Third, the target of estimation is different; we provide p -values to estimate k , while the prior work aims to estimate the eigenvalues of Σ , which is presumed to be full rank.

Since the preprint version of this paper [Chen et al., 2021], related sample-splitting approaches have been developed for settings where traditional sample splitting is infeasible. Neufeld et al. [2024a,b] propose “data thinning” and “count splitting,” methods that decompose individual observations into independent parts for convolution-closed distributions, enabling model validation tasks including dimension selection for low-rank approximations. Baharav et al. [2024] develop finite-sample valid tests for contingency tables using linear test statistics. Most recently, Ancell et al. [2025] apply data thinning to network data, using one network realization to estimate community structure and another to conduct inference—a setting that parallels our use of sample splitting for estimating graph dimension.

For cross-validated eigenvalues, we provide a central limit theorem, which leads to a p -value for the statistical significance of a sample eigenvector. This can be used to estimate the number of statistically useful sample eigenvectors, and thus k . We provide consistency results for the proposed estimator of k , allowing for weighted and sparse graphs. Finally, through simulations and real data applications, we show that this estimator compares favorably to alternative approaches in both computational and statistical performance.

1.3 Prior literature

Numerous methods have been proposed to estimate k under the Stochastic Blockmodel and its degree-corrected version [Bordenave et al., 2015, Bickel and Sarkar, 2016, Lei, 2016, Wang and Bickel, 2017, Chen and Lei, 2018, Ma et al., 2019, Le and Levina, 2019, Liu et al., 2019, Jin et al., 2020]. One previous technique has been proposed to estimate the dimension of the more general random dot product graph [Li et al., 2020]. These methods roughly fall into one of three categories: spectral, cross-validation, and (penalized) likelihood-based approaches. Methods based on likelihood or cross-validation are actively researched, yet the majority of them are commonly restrained by the scale of networks. Spectral methods are highly scalable for estimating k in large networks, although their rigorous analyses require delicate, highly technical random matrix arguments [Ajanki et al., 2017, Benaych-Georges et al., 2019, Chakrabarty et al., 2020, Dumitriu and Zhu, 2019, Benaych-Georges et al., 2020, Hwang et al., 2020].

Among the likelihood-based approaches, the authors of Wang and Bickel [2017] proposed to estimate k by solving a Bayesian information criterion (BIC) type optimization problem, where the objective function is a sum of the log-likelihood and of the model complexity. The computation is often not feasible because the likelihood contains exponentially many terms. In Ma et al. [2019], a pseudo-likelihood ratio is used to compare the goodness-of-fit of models with differing k s that have been estimated using spectral clustering with regularization [Rohe et al., 2011, Qin and Rohe, 2013, Joseph and Yu, 2016, Su et al., 2019], speeding up the computation. However, the two methods allow little node degree heterogeneity. Related to the goodness-of-fit technique, the authors of Jin et al. [2020] present a stepwise testing approach based on the number of quadrilaterals in the networks. Computing the statistic requires at least n^2 multiplication operations, regardless of the sparsity of the graph, thus is infeasible for large n . More recently, cross-validation [Picard and Cook, 1984, Arlot and Celisse, 2010] has also been adapted to the context of choosing k . For example, in Chen and Lei [2018], a block-wise node-pair splitting technique is introduced. In each fold, a block of rows of the adjacency matrix are held out from the Stochastic Blockmodel fitting (including the community memberships), then the left-out rows are used to calculate a predictive loss. In Li et al. [2020], the authors propose to hold out a random fraction of node-pairs, instead of nodes (thus all the incidental node-pairs). In addition, they suggest using a general low-rank matrix completion (e.g., a singular value thresholding approach [Chatterjee, 2015]) to calculate the loss on the left-out node-pairs. Theoretical conditions for not under-estimating k were established in both cross-validation based methods [Chen and Lei, 2018, Li et al., 2020]. Calculating the loss on either held-out rows or on scattered values in the adjacency matrix requires $O(n^2)$ computations, regardless of sparsity. This limits the ability of these techniques to scale to large graphs.

In Bickel and Sarkar [2016], Lei [2016], hypothesis tests using the top eigenvalue or singular value of a properly normalized adjacency matrix are proposed, based on edge universality and other related results for general Wigner ensembles [Tracy and Widom, 1994, Soshnikov, 1999, Erdős et al., 2012, 2013, Alex et al., 2014]. The analyses of these hypothesis tests assume dense graphs. In Liu et al. [2019], a version of the “elbow in the scree plot” approach (see, e.g., Zhu and Ghodsi [2006] for a discussion of this approach) is analyzed rigorously under the Degree-Corrected Stochastic Blockmodel, also in the dense case. For sparser graphs, the spectral properties of other matrices associated to graphs have been used to estimate k , including the non-backtracking matrix [Krzakala et al., 2013, Bordenave et al., 2015, Le and Levina, 2019] and the Bethe-Hessian matrix [Le and Levina, 2019]. However, their theoretical analysis currently allow little node degree heterogeneity in the sparse case.

There is also related work on bootstrapping [Snijders and Borgatti, 1999, Thompson et al., 2016, Green and Shalizi, 2017, Levin and Levina, 2019, Lin et al., 2020a], jackknife resampling [Lin et al., 2020b] and subsampling [Bhattacharyya and Bickel, 2015, Lunde and Sarkar, 2019, Naulet et al., 2021] in network analysis. In particular, in Lunde and Sarkar [2019], subsampling schemes are applied to the nonzero eigenvalues of the adjacency matrix under low-rank graphon models. Weak convergence results are established under some technical conditions, including sufficient edge density (i.e., average degree growing asymptotically faster than \sqrt{n}); simulation results also indicate that sparsity leads to poor performance for the estimators considered, especially in the case of the eigenvalues closer to the bulk.

2 Measuring the signal strength of sample eigenvectors

We consider a connected multigraph $G = (V, E)$ consisting of the set of nodes $V = \{1, \dots, n\}$ and undirected edges E , where we allow multiple edges and self-loops. The *adjacency matrix* $A \in \mathbb{N}^{n \times n}$ records the number of edges between i and j in element A_{ij} . Define the *population (or expectation) matrix* of A as $P = \mathbb{E}(A)$. In this paper, we focus on a simple class of random dot product graphs (see remarks after the definitions).

Definition 1 (Poisson random graph). *Let A be the adjacency matrix of a Poisson random graph. Then, A is symmetric, and the upper-triangular elements of A are independent Poisson random variables, and its population matrix P has the eigendecomposition*

$$P = U\Lambda U^T \tag{1}$$

for $U \in \mathbb{R}^{n \times k}$ with orthonormal columns and diagonal matrix $\Lambda \in \mathbb{R}^{k \times k}$ with positive elements $\lambda_1, \dots, \lambda_k \in \mathbb{R}$ down the diagonal in non-increasing order.

While Definition 1 makes two simplifying assumptions, the method generalizes to graph with various edges, which we remark on in order.

Remark 2.1 (Directed edges). *The first simplifying assumption is that A is symmetric (i.e., edges are undirected). This assumption can be relaxed; Remark 4.4 discusses directed graphs, contingency tables, and rectangular incidence matrices.*

Remark 2.2 (Bernoulli edges). *The second simplifying assumption is that the elements of A are Poisson. It is common to model A_{ij} as Poisson because it is convenient and, in*

sparse graphs specifically, the difference between the Poisson and Bernoulli models becomes negligible [Karrer and Newman, 2011, Flynn et al., 2020, Crane and Dempsey, 2018, Cai et al., 2016, Zhou and Amini, 2020]. Section 3.4 provides the formal extension to Bernoulli graphs via a conditional CLT, with simulations in Supplementary Section S3 demonstrating that the proposed technique provides reliable p-values.

Remark 2.3 (Random dot product model). *The introduction motivated the paper by expressing $\mathbb{E}(A_{ij}) = \langle Z_i, Z_j \rangle = \sum_{\ell=1}^k Z_{i\ell}Z_{j\ell}$, where $Z_i \in \mathbb{R}^k$ is a vector of characteristics for node i . If the $Z_1, \dots, Z_n \in \mathbb{R}^k$ span \mathbb{R}^k and the elements A_{ij} are independent Poisson variables, then this model is included in Definition 1.*

The diagonal of Λ contains the leading k population eigenvalues of P and their corresponding eigenvectors are in the columns of U . For $j > k$, the population eigenvalues of P are $\lambda_j = 0$. In this paper, we aim to estimate the number of nonzero eigenvalues.

2.1 Sample eigenvalues: a poor diagnostic

A common approach to estimating the eigenvalues of P is to use a plug-in estimator, i.e., estimating the eigenvalues of P with the eigenvalues of A . Specifically, for $j = 1, \dots, n$, the j th eigenvectors $\hat{x}_j \in \mathbb{R}^n$ of a symmetric matrix $A \in \mathbb{N}^{n \times n}$ is defined as

$$\hat{x}_j = \operatorname{argmax}_{x \in \hat{S}_j} x^T A x, \tag{2}$$

where $\hat{S}_j = \{x \in \mathbb{R}^n : \|x\|_2 = 1 \text{ and } x^T \hat{x}_\ell = 0 \text{ for } \ell = 1, \dots, j-1\}$. Correspondingly, the objective values for $j = 1, \dots, n$ are called the eigenvalues $\hat{\lambda}_j$,

$$\hat{\lambda}_j = \hat{x}_j^T A \hat{x}_j. \tag{3}$$

The eigenvalues of A , i.e., $\hat{\lambda}_1, \hat{\lambda}_2, \hat{\lambda}_3, \dots$, are often plotted against their index $1, 2, 3, \dots$. This is called a scree plot and it is used as a diagnostic to estimate k (Figure 1). In this scree plot, there might be a “gap” or an “elbow” at the k th eigenvalue, which reveals k .

However, there is an overfitting and bias problem with the plug-in estimator for the population eigenvalues which can make the “gap” or “elbow” in the scree plot more difficult to observe. The leading eigenvalue estimates $\hat{\lambda}_1, \dots, \hat{\lambda}_k$ are asymptotically unbiased, so long as their corresponding population eigenvalues $\lambda_1, \dots, \lambda_k$ are large enough (see, e.g., Chakrabarty et al. [2020] for related results). By contrast, $\lambda_{k+1} = 0$ is not growing; $\hat{\lambda}_{k+1}$ is a biased estimate of $\lambda_{k+1} = 0$, with $\mathbb{E}(\hat{\lambda}_{k+1}) > \lambda_{k+1} = 0$ (see, e.g., Benaych-Georges et al.

[2020] for related results). So, if λ_k is not large enough, then this bias diminishes the appearance of a “gap” or “elbow” between $\hat{\lambda}_k$ and $\hat{\lambda}_{k+1}$ in the scree plot.

This can be seen in the left panel of Figure 2. In that figure, the gap between the sample eigenvalues (black line) and the population eigenvalues (orange line) grows wider as k increases.¹

2.2 Population-validated eigenvalues

Even if an oracle were to tell us that the population eigenvector x_j has population eigenvalue $\lambda_j \neq 0$, we should only use the sample eigenvector \hat{x}_j for statistical inference if \hat{x}_j is close to x_j and other leading population eigenvectors. Because of this requirement, the population eigenvalues λ_j do not measure the signal strength of \hat{x}_j .

In the realistic setting where the signal is not overwhelming for every sample eigenvector \hat{x}_j for $j < k$, we propose to measure the signal strength of this vector in the following way. We define the *population-validated eigenvalue*² of a sample eigenvector \hat{x}_j as

$$\lambda_P(\hat{x}_j) = \hat{x}_j^T P \hat{x}_j. \quad (4)$$

Although this is not an eigenvalue in the traditional sense, there are three reasons to think of this quantity as an analogue.

First, the quadratic form in Equation (4) mimics the form for the sample eigenvalue in Equation (3), which is also the objective function that the sample eigenvectors optimize in Equation (2). As such, for a population eigenvector x_j , $\lambda_P(x_j)$ is the corresponding population eigenvalue λ_j .

The second reason to think of λ_P as an analogue of an eigenvalue is that for a sample eigenvector \hat{x} , there always exists a vector $\hat{x}^\perp \in \mathbb{R}^n$ that is orthogonal to \hat{x} and $P\hat{x} = \hat{\lambda}\hat{x} + \hat{x}^\perp$ for some value $\hat{\lambda} \in \mathbb{R}$. If $\hat{x}^\perp = 0$, then \hat{x} is an eigenvector of P with eigenvalue $\hat{\lambda}$. Even when $\hat{x}^\perp \neq 0$, if $\|\hat{x}\|_2 = 1$, then $\hat{\lambda} = \lambda_P(\hat{x})$. This is because

$$\lambda_P(\hat{x}) = \hat{x}^T P \hat{x} = \hat{x}^T (\hat{\lambda}\hat{x} + \hat{x}^\perp) = \hat{\lambda}$$

The third reason also provides intuition for why λ_P is a measure of signal strength; indeed λ_P provides for the optimal reconstruction of P as conceptualized in the following proposition (a proof is included in Supplementary Section S1 for completeness).

¹In this figure, it is not the eigenvalues of A and $\mathbb{E}(A)$ that are shown, but rather the eigenvalues of the normalized and regularized forms of A and $\mathbb{E}(A)$.

²The notion of $\lambda_P(\hat{x}_j)$ was previously proposed and studied in Abadir et al. [2014] and Lam [2016] for optimal estimation of eigenvalue shrinkage under a different statistical model.

Proposition 2.1 (Lam [2016]). For $j = 1, \dots, q$, $\hat{\lambda}_j = \lambda_P(\hat{x}_j)$ is the solution to

$$\min_{\hat{\lambda}_1, \dots, \hat{\lambda}_q} \left\| P - \sum_{j=1}^q \hat{\lambda}_j \hat{x}_j \hat{x}_j^T \right\|_F.$$

A key advantage of the population quantity $\lambda_P(\hat{x}_j)$ over λ_j is that it reveals information about the vector that we can compute, i.e., \hat{x}_j , not the eigenvector that we wish we had, i.e., x_j . If a sample eigenvector \hat{x}_j is close to its population counterpart x_j , then for the reasons above, it is reasonable to presume that $\lambda_P(\hat{x}_j)$ is close to the population eigenvalue λ_j . However, if the estimation problem is too difficult and \hat{x}_j is nearly orthogonal to the eigenvectors of P that have non-zero eigenvalues, then $\lambda_P(\hat{x}_j) \approx 0$. Notably, and most importantly, this can happen even if \hat{x}_j 's corresponding population eigenvector x_j has a non-zero eigenvalue. For example, this happens when the estimation problem is too difficult as happens for the 60th-128th sample eigenvectors in Figure 2.

3 The three key pieces for cross-validated eigenvalues

It is tempting to compute the eigenvectors \hat{x}_j of A with all of the edges and then choose k based on the population-validated eigenvalues $\lambda_P(\hat{x}_j)$. However, $\lambda_P(\hat{x}_j)$ is not observed (as P is unobserved). In this section, we detail the three key pieces that enable an unbiased estimator of population-validated eigenvalues, which we called *cross-validation eigenvalues*. For cross-validation, we describe an edge splitting procedure to create two Poisson random graphs that are independent and have identical population eigenvectors. The cross-validation eigenvalue is an intuitive plug-in estimator using information from both split graphs, and mostly importantly, it is asymptotically normal.

3.1 The first piece: edge splitting creates independent Poisson graphs

The edge splitting (ES) procedure is described in Algorithm 1. ES splits the edges of a graph into two graphs and outputs the two adjacency matrices \tilde{A} and \tilde{A}_{test} (we omit “train” in \tilde{A}_{train} for simplicity). Notice that under ES and conditionally on A_{ij} , $\tilde{A}_{ij} \sim \text{Binomial}(A_{ij}, 1 - \varepsilon)$ and $[\tilde{A}_{\text{test}}]_{ij} = A_{ij} - \tilde{A}_{ij}$.

For the first piece, the independence of \tilde{A} and \tilde{A}_{test} follows from the next lemma, often referred to as thinning (see, e.g., Durrett [2019, Section 3.7.2]).

Input: adjacency matrix $A \in \mathbb{N}^{n \times n}$ and edge splitting probability $\varepsilon \in (0, 1)$.

Procedure ES(A, ε):

1. Convert A into $G = (V, E)$, where $\{i, j\}$ is repeated in the edge set E potentially more than once if $A_{ij} > 1$.
2. Initiate \tilde{E}_{test} and \tilde{E} , two empty edge sets on V .
3. **for** each copy of edge $\{i, j\} \in E$ **do**
 assign it to \tilde{E}_{test} with probability ε . Otherwise, assign it to \tilde{E} .
4. Convert $(V, \tilde{E}_{\text{test}})$ into an adjacency matrix $\tilde{A}_{\text{test}} \in \mathbb{N}^{n \times n}$ and (V, \tilde{E}) into an adjacency matrix $\tilde{A} \in \mathbb{N}^{n \times n}$

Output: \tilde{A} and \tilde{A}_{test} .

Algorithm 1: Edge splitting

Lemma 3.1. *Define $X \sim \text{Poisson}(\lambda)$ and conditionally on X , define $Y \sim \text{Binomial}(X, p)$ and $Z = X - Y$. Unconditionally on X , the random variables Y and Z are independent Poisson random variables and, further, $Y \sim \text{Poisson}(p\lambda)$ and $Z \sim \text{Poisson}((1 - p)\lambda)$.*

To apply the lemma, let X be A_{ij} , let λ be P_{ij} , let Y and Z be the (i, j) -th elements of \tilde{A} and \tilde{A}_{test} respectively, and let $p = \varepsilon$. This results in the independence between \tilde{A} and \tilde{A}_{test} .

Corollary 3.1. *\tilde{A} and \tilde{A}_{test} are the adjacency matrices of two independent Poisson random graphs, and $\mathbb{E}(\tilde{A}) = (1 - \varepsilon)A$, and $\mathbb{E}(\tilde{A}_{\text{test}}) = \varepsilon A$.*

3.2 The second piece: the splitting population graphs have identical eigenvectors

The next proposition shows that ES preserves the spectral properties of the population adjacency matrices $\mathbb{E}(\tilde{A})$ and $\mathbb{E}(\tilde{A}_{\text{test}})$ from $\mathbb{E}(A)$. This result does not require any distributional assumptions on A , only that its elements are integers (so that \tilde{A} and \tilde{A}_{test} are defined).

Proposition 3.1. *If \tilde{A} and $\tilde{A}_{\text{test}} \in \mathbb{N}^{n \times n}$ are generated by applying ES to $A \in \mathbb{N}^{n \times n}$ with splitting probability ε , then*

1. *The eigenvectors of $\mathbb{E}(A)$, $\mathbb{E}(\tilde{A})$, and $\mathbb{E}(\tilde{A}_{\text{test}})$ are identical.*
2. *If λ_j is an eigenvalue of $\mathbb{E}(A)$, then $(1 - \varepsilon)\lambda_j$ is an eigenvalue of $\mathbb{E}(\tilde{A})$ and $\varepsilon\lambda_j$ is an eigenvalue of $\mathbb{E}(\tilde{A}_{\text{test}})$.*

Here, all expectations are unconditional on A .

Proof. Define $P = \mathbb{E}(A)$ and let $P = U\Lambda U^T$ be its eigendecomposition; if A is not random, then $P = A$ and U, Λ potentially have n columns. It follows directly from the construction in ES that $\mathbb{E}(\tilde{A}) = (1 - \varepsilon)P$ and $\mathbb{E}(\tilde{A}_{\text{test}}) = \varepsilon P$. Rearranging terms reveals the eigendecomposition of $\mathbb{E}(\tilde{A}_{\text{test}})$,

$$\mathbb{E}(\tilde{A}_{\text{test}}) = \varepsilon P = U(\varepsilon\Lambda)U^T$$

and similarly for $\mathbb{E}(\tilde{A})$. This shows that they have the same eigenvectors and the simple relationship between their eigenvalues in the statement. \square

By making ε small we can ensure that the subsampled eigenvectors \tilde{x}_j are nearly as good as \hat{x}_j . Without loss of generality, let \tilde{x} be any eigenvector of \tilde{A} . We define the *cross-validated eigenvalues* as

$$\lambda_{\text{test}}(\tilde{x}) = \tilde{x}^T \tilde{A}_{\text{test}} \tilde{x}.$$

This estimator is a weighted sum of quantities from both split graphs that are independent and have identical population eigenvectors.

3.3 The third piece: the cross-validated eigenvalues are asymptotically normal

In this section, we provide a central limit theorem (CLT) for $\lambda_{\text{test}}(\tilde{x})$. We define the sample and population total variance as

$$\hat{\sigma}^2 = 2(\tilde{x}^2)^T \tilde{A}_{\text{test}}(\tilde{x}^2) - (\tilde{x}^2)^T \text{diag}(\tilde{A}_{\text{test}})(\tilde{x}^2)$$

and

$$\sigma^2 = 2(\tilde{x}^2)^T (\varepsilon P)(\tilde{x}^2) - (\tilde{x}^2)^T \text{diag}(\varepsilon P)(\tilde{x}^2).$$

Next, we define the following delocalization condition on \tilde{x} :

$$\|\tilde{x}\|_{\infty}^2 = o(\sigma) \tag{5}$$

where $\tilde{x}^2 \in \mathbb{R}^n$ is the vector x with all entries squared.

Theorem 3.1 (CLT for cross-validated eigenvalues). *Assume that \tilde{x} satisfies the delocalization condition (5). Then,*

$$\frac{\lambda_{\text{test}}(\tilde{x}) - \lambda_{\varepsilon P}(\tilde{x})}{\hat{\sigma}} \Rightarrow N(0, 1). \tag{6}$$

The proof of Theorem 3.1 is in Supplementary Section S1. When \tilde{x} is the eigenvector of \tilde{A} 's normalized form, a similar CLT result exists.

Remark 3.1 (Sufficient condition). *Regarding the delocalization condition (5), when all entries of εP are of the same order $\rho = o(1)$, then $\sigma = \Theta(\rho^{1/2})$ and the condition boils down to $\|x\|_\infty = o(\rho^{1/4})$. In Supplementary Section S1.2.2 (Corollary S1.1), we discuss a sufficient condition for $\|x\|_\infty^2 = o(\sigma)$ to hold in terms of the expected number of edges in \tilde{A}_{test} .*

Remark 3.2 (Bernoulli graphs). *Algorithm 2 operates identically for Bernoulli graphs. While the theoretical justification requires conditioning on the edge-splitting pattern (Section 3.4), this conditioning is implicit in the randomization and does not affect the implementation.*

Based on Theorem 3.1, we test the null hypothesis that the expected value of $\lambda_{\text{test}}(\tilde{x})$ is zero,

$$H_0 : \lambda_{\varepsilon P}(\tilde{x}) = 0$$

Note that the null is equivalent to population-validate eigenvalue $\lambda_P(\tilde{x})$ is zero, since $\varepsilon > 0$ is a constant. Under the null, \tilde{x} is orthogonal to the latent space; in this case, we say that \tilde{x} is not statistically useful (although, perhaps, it is still useful for tasks other than estimating graph dimension k).

3.4 Extension to Bernoulli graphs

While the three key pieces presented above provide clean intuition and theory for Poisson graphs, extending to Bernoulli graphs requires a modified approach. The fundamental challenge is that Lemma 3.1, which guarantees the independence between \tilde{A} and \tilde{A}_{test} under edge splitting for Poisson graphs, has no counterpart for Bernoulli graphs; when $A_{ij} \in \{0, 1\}$, an edge cannot simultaneously appear in both \tilde{A} and \tilde{A}_{test} , creating a negative dependence.

To generate an “independent copy” in the Bernoulli case, we instead split possible edges; let $\Omega \subseteq \{(i, j) : 1 \leq i < j \leq n\}$ be a random subset of all $\binom{n}{2}$ possible edges, where each pair is included in Ω independently with probability ε . This set Ω determines which edges are *eligible* for the test set, regardless of whether they appear in the observed graph. Conditionally on Ω , we define:

$$[\tilde{A}_{\text{test}}^\Omega]_{ij} \stackrel{\text{ind.}}{\sim} \text{Bernoulli}([P_\Omega]_{ij}), \tag{7}$$

$$[\tilde{A}^\Omega]_{ij} \stackrel{\text{ind.}}{\sim} \text{Bernoulli}([P - P_\Omega]_{ij}). \tag{8}$$

where $[P^\Omega]_{ij} = P_{ij}$ if edge $(i, j) \in \Omega$ otherwise 0. Given Ω , $\tilde{A}_{\text{test}}^\Omega$ and \tilde{A}^Ω are conditionally independent. For example, if $\tilde{x} \in \mathbb{R}^n$ is an eigenvector of \tilde{A}^Ω , then \tilde{x} and $\tilde{A}_{\text{test}}^\Omega$ are conditionally independent given Ω .

Crucially, Algorithm 1 (ES) provides an efficient implementation of this conditioning. Rather than explicitly generating Ω for all $O(n^2)$ possible edges, ES only processes the observed edges in A , which is $O(m)$ where m is the number of edges. The resulting split is distributionally equivalent to first sampling Ω , then generating the conditional graphs. Thus, the computational efficiency of the algorithm remains unchanged. Under this conditioning, we have the following result (the proof is in Supplementary Section S1):

Theorem 3.2 (Conditional CLT for Bernoulli graphs). *Assume $\max_{i,j} P_{ij} = o(1)$. Suppose that with probability 1, a unit vector \tilde{x} satisfies the delocalization condition $\|\tilde{x}\|_\infty^2 = o(\sigma_\Omega)$, where the population total variance is*

$$\sigma_\Omega^2 = 2(\tilde{x}^2)^\top (P_\Omega - P_\Omega^2)\tilde{x}^2 - (\tilde{x}^2)^\top \text{diag}(P_\Omega - P_\Omega^2)\tilde{x}^2$$

with $[P_\Omega^2]_{ij} = [P_\Omega]_{ij}^2$ for simplicity, and that $\sigma_\Omega > 0$ eventually. Then, conditionally on Ω ,

$$\frac{\lambda_{\text{test}}^\Omega(\tilde{x}) - \lambda_{P_\Omega}\tilde{x}}{\hat{\sigma}_\Omega} \Rightarrow N(0, 1), \quad \text{almost surely,}$$

where $\lambda_{\text{test}}^\Omega(\tilde{x}) = \tilde{x}^\top \tilde{A}_{\text{test}}^\Omega \tilde{x}$ and $\hat{\sigma}_\Omega^2 = 2(\tilde{x}^2)^\top \tilde{A}_{\text{test}}^\Omega \tilde{x}^2 - (\tilde{x}^2)^\top \text{diag}(\tilde{A}_{\text{test}}^\Omega)\tilde{x}^2$ is the sample variance estimate.

The variance formula σ_Ω^2 includes terms $(1 - [P_\Omega]_{ij})$ reflecting the Bernoulli structure, in contrast to the Poisson case in Theorem 3.1. Since $(1 - [P_\Omega]_{ij}) \leq 1$, the Poisson variance formula provides an upper bound, enabling conservative inference.

This theoretical modification has two practical implications. First, Algorithm 2 (EigCV) operates identically for both Poisson and Bernoulli graphs—the conditioning is implicit in the randomization. Second, the negative dependence makes the test conservative, particularly for denser graphs where more edges create more dependence. As demonstrated in Supplementary Section S3, this conservativeness is most pronounced in denser graphs, for eigenvectors beyond the true dimension k . Despite reduced power, this conservativeness maintains valid inference, making the method reliable for the Bernoulli graphs that arise in practice.

Our main consistency result (Theorem 4.1) in the next section extends to the Bernoulli case with minor modifications (see Supplementary Remark S1.1), where εP is replaced with the conditional expectation. Thus, our method provides both valid inference and consistent

estimation of k for Bernoulli graphs, with the primary cost being conservative p -values that may reduce power in dense graphs.

4 Cross-validated eigenvalue estimation

In this section, we use Theorem 3.1 to test the null hypothesis $H_0 : \lambda_P(\tilde{x}_j) = 0$, where \tilde{x}_j is the j th eigenvector of \tilde{A} . Ideally, the first k eigenvectors will provide large values of $\lambda_{\text{test}}(\tilde{x}_j)$ for $j = 1, 2, \dots, k$, while the following eigenvectors have $\lambda_{\text{test}}(\tilde{x}_j) \approx 0$ for $j > k$, whose Z -scores distributed normally around zero (with variance one). Section 4.1 states the algorithm and Section 4.2 provides the main theoretical result, i.e., this estimation is consistent.

4.1 The algorithm

Algorithm 2 revokes ES and calculated up to k_{\max} cross-validated eigenvalues. The algorithm reports a p -value for each eigenvector. These are then used to estimate k . For simplicity, we describe the algorithm for an undirected graph with the adjacency matrix $A \in \mathbb{N}^{n \times n}$; see Remark 4.4 for rectangular or asymmetric A .

In Algorithm 2, we allow for several algorithmic modifications from the main statistical theory in Section 4.2 (Theorem 4.1) because they are practically advantageous. These include repetition of cross-validation (Step 1), graph Laplacian (Step 1b), and a delocalization check. We discuss the choices in order.

Remark 4.1 (Repetition of cross-validation). *Increasing $n_{cv} > 1$ helps to remove the randomness in the p -values generated from edge splitting ES (see Supplementary Section S3.2 for further discussion of folds > 1).*

Remark 4.2 (Graph Laplacian). *While the technical parts of the paper use the eigenvectors of an adjacency matrix, the proposed algorithm instead uses eigenvectors from the normalized and regularized adjacency matrices. Importantly, the normalized and regularized form of $\mathbb{E}(A)$ has the same number k of non-zero eigenvalues as $\mathbb{E}(A)$. For dense graphs, L has similar statistical properties to A . However, for sparse graphs, L helps reduces localization of eigenvectors [Le et al., 2017, Zhang and Rohe, 2018].*

Remark 4.3 (Check for delocalization). *Finally, there is an additional step needed in Theorem 4.1 to check for delocalization. This technical requirement is further discussed in Section 4.2. This step is not used in EigCV or in our implementation. We do not include a check for delocalization because we find in the simulation in Supplementary Section S3*

Input: symmetric adjacency matrix $A \in \mathbb{N}^{n \times n}$, edge splitting probability

$\varepsilon \in (0, 1)$, maximum possible graph dimension $k_{\max} > 1$

Optional Input: number of cross-validation repetitions n_{cv} (default to 10), and significance level α (default to 0.05)

Procedure $\text{EigCV}(A, \varepsilon, k_{\max}, \alpha, n_{\text{cv}})$:

1. **for** $i = 1, \dots, n_{\text{cv}}$ **do**

a. $\tilde{A}, \tilde{A}_{\text{test}} \leftarrow \text{ES}(A, \varepsilon)$

// Algorithm 1

b. (Optional) Compute graph Laplacian \tilde{L} with \tilde{A} ,

$$\tilde{L} = \tilde{D}\tilde{A}\tilde{D},$$

where $\tilde{D} \in \mathbb{R}^{n \times n}$ is a diagonal matrix with element $\tilde{D}_{ii} = (\tilde{d}_i + \tilde{\tau})^{-1/2}$ and node degrees $\tilde{d}_i = \sum_j \tilde{A}_{ij}$ and regularization parameter $\tilde{\tau} = \sum_i \tilde{d}_i/n$.

c. Compute the leading k_{\max} eigenvectors of \tilde{L} (or \tilde{A}), as $\tilde{x}_1, \dots, \tilde{x}_{k_{\max}}$.

d. **for** $j = 2, \dots, k_{\max}$ **do**

Compute the test statistic

$$T_{f,j} = \frac{\lambda_{\text{test}}(\tilde{x}_j)}{\hat{\sigma}_j},$$

where $\lambda_{\text{test}}(\tilde{x}) = \tilde{x}^T \tilde{A}_{\text{test}} \tilde{x}$, and $\hat{\sigma}_j = \sqrt{2\varepsilon(\tilde{x}_j^2)^T A \tilde{x}_j^2 - \varepsilon(\tilde{x}_j^2)^T \text{diag}(A) \tilde{x}_j^2}$ is the standard error evaluated using the full graph, and \tilde{x}_j^2 is the vector \tilde{x}_j with each element squared.

2. **for** $j = 2, \dots, k_{\max}$ **do**

Compute T_j as the mean of the $T_{1,j}, \dots, T_{n_{\text{cv}},j}$ and compute the one-sided

p -value $p_j = 1 - \Phi(T_j)$, where Φ is the cumulative distribution function of the standard normal distribution.

Output: The graph dimensionality estimate: $\text{argmin}_{k \leq k_{\max}} \{p_k \geq \alpha\} - 1$.

Algorithm 2: Eigenvalue cross-validation

that when an eigenvector \tilde{x}_j delocalizes, $(\tilde{x}_j^2)^\top A \tilde{x}_j^2$ in the formula for $\hat{\sigma}_j$ is very large, thus leading to conservative inferences.

Algorithm 2 (**EigCV**) operates identically for Bernoulli graphs. Furthermore, the framework of **EigCV** easily extends to two other settings, rectangular incidence matrices and a test of independence for contingency tables. We remark on the two extensions in order.

Remark 4.4 (Rectangular incidence matrices). *If the matrix $A \in \mathbb{N}^{r \times c}$ is either rectangular or asymmetric (e.g., the adjacency matrix for a directed graph, the incidence matrix for a bipartite graph, a contingency table, etc.), then eigenvectors should be replaced by singular vectors. In Step 1c of **EigCV**, compute the singular vector pairs \tilde{u}_j and \tilde{v}_j . Then, the define test statistic in Step 1d as*

$$T_j = \frac{\tilde{u}_j^\top \tilde{A}_{\text{test}} \tilde{v}_j}{\sqrt{\varepsilon(\tilde{u}_j^2)^\top A \tilde{v}_j}}.$$

Theorem 3.1 extends under analogous conditions to this setting. Our R package, `gdim` (available from CRAN), includes this extension.

Remark 4.5 (Contingency tables). *Suppose $A \in \mathbb{N}^{r \times c}$ is a contingency table with multinomial elements. Note that the χ^2 test of independence tests the null hypothesis that $\mathbb{E}(A)$ is rank 1, i.e., $k = 1$. To test if $\mathbb{E}(A)$ has rank greater than $k = 1$ and potentially reject independence, one can apply **EigCV** to A with $k_{\max} = 2$, using the extension to rectangular matrices in Remark 4.4. The three key pieces for the cross-validation apply to this setting, thus enabling this approach. First, if the distribution of A is multinomial, then **ES** provides two independent matrices. Second, in expectation, those matrices have identical singular vectors and the same number of non-zero singular values. Third, the CLT in Theorem 3.1 extends to this data generating model with analogous conditions. **EigCV** is potentially powerful for alternative hypotheses where $\mathbb{E}(A)$ has a large second eigenvalue. In contrast to the traditional Pearson's χ^2 test for independence, **EigCV** handles a large number of rows and columns and a sparse A , where the vast majority of elements are zeros. Moreover, it has the added advantage that the singular vectors \tilde{u}_2 and \tilde{v}_2 estimate where the deviation from independence occurs, thus making the results more interpretable. This is an area of our ongoing research.*

4.2 Statistical consistency

This section states a consistency result for a modified version of the algorithm stated in Algorithm S1 in Supplementary Section S1.3. The main modification is the addition of a delocalization test. We use K for the true latent dimension and \hat{K} for its estimate.

We will make some further assumptions. Let $P = \rho_n P^0$, where $0 < \rho_n < 1$ controls the sparsity of the network, and $P^0 = U \Lambda^0 U^T$ is a matrix of rank k with $P_{ij}^0 \leq 1$ for all i, j . Here, $\Lambda^0 = \text{diag}(\lambda_1^0, \dots, \lambda_K^0)$ is the diagonal matrix of its non-increasing eigenvalues, and $U = (u_1, \dots, u_K)$ contains the corresponding eigenvectors. We first consider the signal strength in the population adjacency matrix. The magnitude of the leading eigenvalues characterize the useful signal in the data; only if they are sufficiently large is it possible to identify them from a finite graph sample. As such, the first assumption requires that the leading eigenvalues of the population graph are of sufficient and comparable magnitude. We also include necessary assumptions on the sparsity of the graph.

Assumption 1 (Signal strength and sparsity). *We assume that there exist positive constants ψ_1, ψ'_1 such that*

$$\kappa := \lambda_1^0 / \lambda_K^0 \in (0, \psi_1), \quad \lambda_1^0 \geq \psi'_1 n.$$

In addition, we assume that $P_{ij}^0 \leq 1$ for all i, j and that the network sparsity satisfies $c_0 \frac{\log \xi_0 n}{n} \leq \rho_n \leq c'_0 n^{-\xi_1}$, for some constants $\xi_0 > 2$, $\xi_1 \in (0, 1)$, $c_0, c'_0 > 0$.

Observe that Assumption 1 implies in particular that $\psi_1^{-1} \psi'_1 n \rho_n \leq \lambda_K \leq \lambda_1 \leq n \rho_n$ since $\lambda_1 \leq \text{tr}(P) \leq n \rho_n$. Assumption 1 is less strict than the assumptions in Li et al. [2020]. This is because we do not require a minimum gap between distinct eigenvalues, which is hard to satisfy in practice.

Next, we consider a property of the population eigenvectors. The notion of coherence was previously introduced by Candès and Recht [2009]. Under the parametrization of Assumption 1, the coherence of U is defined as

$$\mu(U) = \max_{i \in [n]} \frac{n}{K} \|U^T e_i\|^2 = \frac{n}{K} \|U\|_{2, \infty}^2,$$

where e_i is the i -th standard basis vector. A lower coherence indicates that the population eigenvectors are more spread-out—that is, they are not concentrated on a few coordinates.

Assumption 2 (Coherence). *We assume $\mu(U) \leq \mu_0$, for some constant $\mu_0 > 1$.*

Our main theoretical result asserts the consistency of our cross-validated eigenvalue estimator for estimating the latent dimension. The proof of Theorem 4.1 is in Supplementary Section S1.

Theorem 4.1 (Consistency). *Suppose $A \in \mathbb{R}^{n \times n}$ is a Poisson graph satisfying Assumptions 1 and 2. Let K be the true latent space dimension, and let \hat{K} be the output of*

Algorithm S1 (see Supplementary Section S1.3) with edge splitting probability ε . Then,

$$\mathbb{P}\left(\hat{K} = K\right) \rightarrow 1 \quad \text{as } n \rightarrow \infty.$$

5 Comparing to other approaches

This section compares the proposed method (**EigCV**) with some existing graph dimensionality estimators using both simulated and real graph data. An **R** implementation of **EigCV** is available from the CRAN package **EigCV**. Throughout, we set the graph splitting probability ε to 0.05, set the significance level cut-off at $\alpha = 0.05$, and $n_{\text{cv}} = 10$.

We compare **EigCV** to (1) BHMC, a spectral method based on the Bethe-Hessian matrix with correction [Le and Levina, 2019]; (2) LR, a likelihood ratio method adapting a Bayesian information criterion [Wang and Bickel, 2017]; (3) ECV, an edge cross-validation method with an area under the curve criterion [Li et al., 2020]; (4) NCV, a node cross-validation using an binomial deviance criterion [Chen and Lei, 2018]; and (5) StGoF (with $\alpha = 0.05$), a stepwise goodness-of-fit estimate [Jin et al., 2020]. We performed all computations in **R**. For (1)-(4), we invoked the **R** package **randnet**, and for (5), we implemented the original Matlab code (shared by the authors) in **R**.

5.1 Numerical experiments

This section presents several simulation studies that compare our method with other approaches to graph dimensionality. We sampled random graphs with $n = 2,000$ nodes and $k = 10$ blocks from the Degree-Corrected Stochastic Blockmodel (DCSBM). Specifically, for any $i, j = 1, 2, \dots, n$,

$$A_{ij} \stackrel{\text{ind.}}{\sim} \text{Bernoulli}\left(\theta_i \theta_j B_{z(i)z(j)}\right),$$

where $z(i) \in \{1, 2, \dots, k\}$ is the block membership of node i , and $B \in \mathbb{R}^{k \times k}$ is the block connectivity matrix, with $B_{ii} = 0.28$ and $B_{ij} = 0.08$ for $i, j = 1, 2, \dots, k$, and $\theta_i > 0$ is the degree parameters of node i . We investigated the effects of degree heterogeneity by drawing θ_i 's from three distributions (before scaling to unit sum): (i) a point mass distribution, (ii) an Exponential distribution with rate 5, (iii) a Pareto distribution with location parameter 0.5 and dispersion parameter 5. From (i) to (iii), the node degrees become more heterogeneous. Finally, to examine the effects of sparsity, we chose the expected average node degree in $\{25, 30, \dots, 60\}$. For each simulation setting, we evaluated all methods 100 times.

Figure 4 displays the accuracy of all graph dimensionality methods. Here, the accuracy

is the fraction of times an estimator successfully identified the true underlying graph dimensionality (which is 10).³ From the results, both BHMC and ECV offered satisfactory estimation when the graph is degree-homogeneous and the average degree becomes sufficiently large, while they were affected drastically by the existence of degree heterogeneity. The LR estimate was affected by degree heterogeneity as well (although less than BHMC or ECV) and also required a relatively large average node degree to estimate the graph dimensionality. The NCV methods failed to estimate the graph dimensionality under most settings. The StGoF estimate worked better for degree-heterogeneous graphs but required a larger average node degree for accuracy. It is also worth pointing out that the LR and StGoF methods tended to over-estimate the graph dimensionality when the average degree is large, especially for the power-law graphs (see Supplementary Figure S7). Finally, our method provided a much more accurate dimensionality estimate overall, requiring smaller average node degree and allowing degree heterogeneity. In addition, our testing approach also enjoys a strong advantage of reduced computational cost. To show this, Figure 5 depicts the average runtime for each method. It can be seen that the proposed method and BHMC are faster than competing methods by several orders of magnitude. The computational complexity of each StGoF iteration (or test) is at least $O(n^2)$, regardless of whether the graph is sparse or not. Consequently, StGoF requires the longest runtime.

5.2 Email network

A real data network was generated using email data within a large European research institution, with each node representing one of the 1005 core members [Leskovec et al., 2007]. There is an edge from node i to node j , if i sent at least one email to j . The dataset also contains 42 “ground-truth” community memberships of the nodes. That is, each individual belongs to exactly one of 42 departments at the research institute. For simplicity, we removed the 14 small departments that consist of less than 10 members (see Supplementary Table S1 for similar results without the filter). This resulted in a directed and unweighted network with a total of 936 nodes from 28 communities.

We applied the graph dimensionality methods to estimate the number of clusters in the network. For the randomized methods (including ECV, NCV, and our proposed method), we ran them 25 times and report the mean and standard deviation of the estimates. For the methods that report a p -value (including StGoF and our proposed method), we use a significance level of $\alpha = 0.01$, followed by a multiplicity correction using the procedure of Benjamini and Hochberg [1995]. We set $k_{\max} = 50$. Finally, we chose the splitting

³Besides comparison of accuracy, we also compared the deviation of the estimation by each method, for which similar results hold consistently (see Supplementary Figure S7).

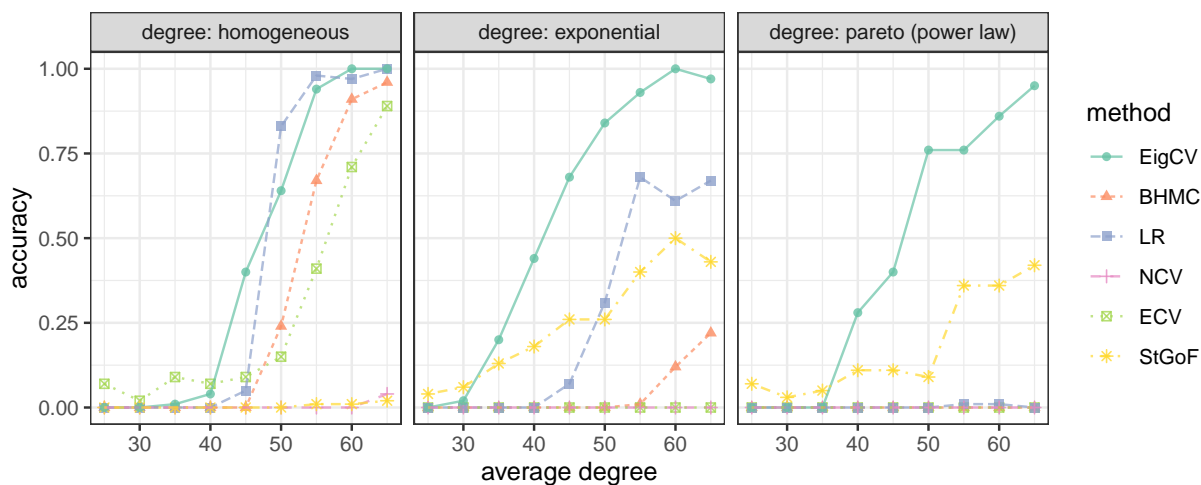


Figure 4: Comparison of accuracy for different graph dimensionality estimates under the DCSBM. The panel strips on the top indicate the node degree distribution used. Within each panel, each colored line depicts the relative error of each estimation method as the average node degree increases. Each point on the lines are averaged across 100 repeated experiments.

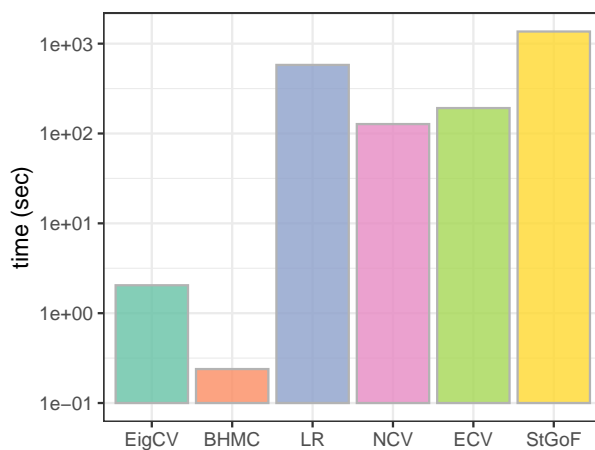


Figure 5: Comparison of runtime for the different graph dimensionality methods. Each colored bar indicates the runtime of applying each method on a DCSBM graph with 2000 nodes and 10 blocks. The maximum graph dimensionality is set to 15 for all methods. The runtime was averaged across 100 repeated experiments.

probability to be 0.05, as the network is sparse with an average node degree of 23.5. Table 1 lists the inferences made by each method. As shown, our method provided an estimate that is close to the true number of departments within the institute. BHMC, LR, NCV, and ECV all estimated small numbers of clusters, while StGoF went significantly larger (≥ 50). These observations were consistent with the simulation results (see Supplementary Figure S7). Among all the others, only the proposed method provided a close estimate (≈ 28) to the true number of departments. Similarly to the simulation results, the BHMC method and our method are more computationally efficient, with much shorter runtime than the others.

Table 1: Comparison of graph dimensionality estimates using the email network among members in a large European research institution. Each members belongs to one of 28 departments.

Method	Estimate (mean)	Runtime (second)
EigCV	28.3	0.68
BHMC	14	0.02
LR	17	85.19
NCV	6.5	204.97
ECV	16.5	41.07
StGoF	≥ 50	397.47

6 Discussion

In this paper, we proposed a new way to estimate the number of latent dimensions in a graph k using the concept of cross-validated eigenvalues. Through edge splitting and thanks to a simple central limit theorem (or conditional CLT for Bernoulli graphs), the estimation of cross-validated eigenvalues is efficient for very large graphs. The paper also provides theoretical justification showing that the estimator is consistent. Our simulations and empirical data application validate the theory and further demonstrate the efficacy of the proposed method.

In addition to being quickly computable, a key advantage of cross-validated eigenvalues is our rigorous understanding of their behavior outside of the asymptotic setting where all k dimensions can be estimated. Theorem 3.1 encodes this rigorous understanding into a p -value. This theorem requires very little of the population matrix P ; it does not presume that it is from a Degree-Corrected Stochastic Blockmodel, nor does it presume the actual rank of P or the order of the eigenvalue being tested. Of course, this level of ease and generality

comes with a price. For Bernoulli graphs specifically, the inference is conservative rather than exact, though still valid. In addition, we only get to compute the eigenvectors with $1 - \varepsilon$ fraction of the edges. The natural possibility is to estimate k with a fraction of the edges and then recompute the eigenvectors with the full graph. Going forward, we hope others will join us in crafting new estimators for $\lambda_P(\hat{x}_j)$ that do not require leaving out edges.

Acknowledgments

This research is partially supported by the National Science Foundation under Grant DMS-1612456 (to K.R.), DMS-1916378 (to S.R. and K.R.), CCF-1740707 (TRIPODS Phase I) and DMS-2023239 (TRIPODS Phase II), and the Army Research Office under Grant W911NF-15-1-0423 (to K.R.). We thank Sündüz Keleş, Po-Ling Loh, Michael A Newton, Kris Sankaran, Muzhe Zeng, Alex Hayes, E Auden Krauska, Sijia Fang, and Jitian Zhao for all the helpful discussions.

Supplementary Materials

S1 Technical proofs

S1.1 Proof of Proposition 2.1

Proof. Let $\hat{X} \in \mathbb{R}^{n \times q}$ contain the leading q sample eigenvectors $\hat{x}_1, \dots, \hat{x}_q$ in its columns.

We aim to show that

$$\min_{\Gamma \text{ is diagonal}} \|P - \hat{X}\Gamma\hat{X}^T\|_F$$

contains $\lambda_P(\hat{x}_1), \dots, \lambda_P(\hat{x}_q)$ down the diagonal.

Using the symmetry of P and the cyclic property of the trace, we obtain

$$\begin{aligned} \|P - \hat{X}\Gamma\hat{X}^T\|_F^2 &= \text{tr}(P^2) + \text{tr}(\hat{X}\Gamma^2\hat{X}^T) - 2\text{tr}(P\hat{X}\Gamma\hat{X}^T) \\ &= \text{tr}(P^2) + \text{tr}(\Gamma^2) - 2\text{tr}(\hat{X}^T P \hat{X} \Gamma). \end{aligned}$$

Taking a derivative with respect to the diagonal of Γ and setting equal to zero gives

$$\Gamma = \text{diag}(\hat{X}^T P \hat{X})$$

which contains $\lambda_P(\hat{x}_1), \dots, \lambda_P(\hat{x}_q)$ down the diagonal. □

S1.2 Proof of asymptotic normality

This section proves the two versions of the central limit theorem (CLT) and a sufficient condition described in Section 3.

S1.2.1 CLT in the Poisson case

Proof of Theorem 3.1. We first show the CLT with the population total variance σ^2 (in the denominator),

$$\frac{\lambda_{\text{test}}(\tilde{x}) - \lambda_{\varepsilon P}(\tilde{x})}{\sigma} \Rightarrow N(0, 1). \quad (\text{S9})$$

by verifying Lyapunov's condition. Then, we show the CLT holds when replacing population variance with the sample total variance $\hat{\sigma}$ via Slutsky's Lemma.

Since \tilde{A}_{test} is symmetric, only the triangular elements are independent. That is, for all $i \leq j$, $[\tilde{A}_{\text{test}}]_{ij}$ are independent. For any $1 \leq i \leq j \leq n$, define random variables $X_{ij} = x_i x_j ([\tilde{A}_{\text{test}}]_{ij} - \varepsilon P_{ij})(2 - \mathbf{1}(i = j))$, where $\mathbf{1}(\cdot)$ is the indicator function. Then, X_{ij} has mean zero and variance $\tilde{x}_i^2 \tilde{x}_j^2 (\varepsilon P_{ij})(2 - \mathbf{1}(i = j))^2$. Furthermore, the numerator in Equation (S9) can be written as the sum of X_{ij} 's, $\lambda_{\text{test}}(\tilde{x}) - \lambda_{\varepsilon P}(\tilde{x}) = \sum_{i \leq j} X_{ij}$. The sum of X_{ij} 's variances is equal to the definition of σ^2 ,

$$\sum_{i \leq j} \tilde{x}_i^2 \tilde{x}_j^2 (\varepsilon P_{ij})(2 - \mathbf{1}(i = j))^2 = 2(\tilde{x}^2)^{\text{T}}(\varepsilon P)(\tilde{x}^2) - (\tilde{x}^2)^{\text{T}} \text{diag}(\varepsilon P)(\tilde{x}^2) = \sigma^2.$$

We verify the fourth moment Lyapunov's condition on the summation of X_{ij} for $i \leq j$ (see, e.g., Durrett [2019, Exercise 3.4.12]).

$$\begin{aligned} & \frac{\sum_{i \leq j} \mathbb{E} \left| \tilde{x}_i \tilde{x}_j ([\tilde{A}_{\text{test}}]_{ij} - \varepsilon P_{ij})(2 - \mathbf{1}(i = j)) \right|^4}{\sigma^4} \\ & \stackrel{(i)}{\leq} \frac{\sum_{i \leq j} (\tilde{x}_i \tilde{x}_j)^4 (4\varepsilon P_{ij})(2 - \mathbf{1}(i = j))^4}{\sigma^4} \\ & \leq \frac{16 \|\tilde{x}\|_{\infty}^4 \sum_{i \leq j} \tilde{x}_i^2 \tilde{x}_j^2 (\varepsilon P_{ij})(2 - \mathbf{1}(i = j))^2}{\sigma^4} \\ & = \frac{16 \|\tilde{x}\|_{\infty}^4}{\sigma^2} \\ & \stackrel{(ii)}{=} o(1), \end{aligned}$$

where (i) comes from the fourth central moment of Poisson variable, $\mathbb{E}([\tilde{A}_{\text{test}}]_{ij} - \varepsilon P_{ij})^4 = \varepsilon P_{ij}(1 + 3\varepsilon P_{ij}) \leq 4\varepsilon P_{ij}$, combining the assumption $\varepsilon P_{ij} \leq 1$, and (ii) is due to the delocal-

ization condition. This shows Equation (S9).

Via Slutsky's Lemma, we can multiply the ratio in Equation (S9) by any sequence that converges to one in probability and the result still holds. The proof is then concluded by showing that $\sigma/\hat{\sigma}$ converges to one in probability. Indeed, we have

$$\begin{aligned}
\text{Var}\left(\frac{\hat{\sigma}^2}{\sigma^2}\right) &= \frac{\text{Var}(\hat{\sigma}^2)}{\sigma^2} \\
&= \frac{\text{Var}\left(2(\tilde{x}^2)^\top \tilde{A}_{\text{test}}(\tilde{x}^2) - (\tilde{x}^2)^\top \text{diag}(\tilde{A}_{\text{test}})(\tilde{x}^2)\right)}{\sigma^4} \\
&= \frac{\text{Var}\left(\sum_{i \leq j} \tilde{x}_i^2 \tilde{x}_j^2 [\tilde{A}_{\text{test}}]_{ij} (2 - \mathbf{1}(i = j))^2\right)}{\sigma^4} \\
&\stackrel{\text{(i)}}{=} \frac{\sum_{i \leq j} \tilde{x}_i^4 \tilde{x}_j^4 \varepsilon P_{ij} (2 - \mathbf{1}(i = j))^4}{\sigma^4} \\
&\leq \frac{4\|\tilde{x}\|_\infty^4 \sum_{i \leq j} \tilde{x}_i^2 \tilde{x}_j^2 \varepsilon P_{ij} (2 - \mathbf{1}(i = j))^2}{\sigma^4} \\
&= \frac{4\|\tilde{x}\|_\infty^4}{\sigma^2} \\
&\stackrel{\text{(ii)}}{=} o(1),
\end{aligned}$$

where (i) is due to the mutual independence among upper triangular elements of \tilde{A}_{test} , and (ii) is due to the delocalization condition. So, by Chebyshev's inequality, $\hat{\sigma}^2/\sigma^2$ converges in probability to its expectation. Note that $\mathbb{E}(\hat{\sigma}^2/\sigma^2) = 1$ and that taking the inverse and the square root is continuous transformation. So, the ratio $\sigma/\hat{\sigma}$ converges in probability to one. \square

S1.2.2 A sufficient condition of CLT in the Poisson case

The following corollary gives a sufficient condition for $\|\tilde{x}\|_\infty^2 = o(\sigma)$ to hold in terms of m and the expected number of edges in \tilde{A}_{test} .

Corollary S1.1. *Using the setting of Theorem 3.1, let $\pi \in \mathbb{R}^n$ be a probability distribution on the nodes with π_i proportional to a node's expected degree. Define $\langle \pi, x^2 \rangle$ be the expected value of x_I^2 for I drawn from π and define $m = \sum_i d_i/2$ as the expected total number of*

edges. If P is positive semi-definite and

$$\frac{\|\tilde{x}\|_\infty^2}{\langle \pi, \tilde{x}^2 \rangle} = o(\sqrt{m}),$$

then the CLT in Equation (6) holds.

Proof. The proof of Corollary S1.1 follows directly from the next lemma.

Lemma S1.1. *Suppose $Q \in \mathbb{R}_+^{n \times n}$ is positive semi-definite. Define $d = Q\mathbf{1}_n \in \mathbb{R}^n$ to be the expected degrees of the nodes $1, \dots, n$, where $\mathbf{1}_n \in \mathbb{R}^n$ is a vector of 1's. Then,*

$$\sigma^2 = 2(\tilde{x}^2)^\top Q \tilde{x}^2 - (\tilde{x}^2)^\top \text{diag}(Q) \tilde{x}^2 \geq \frac{\langle d, \tilde{x}^2 \rangle^2}{\sum_i d_i}.$$

Proof. Define $y = \tilde{x}^2$, $\theta = d^{1/2}$, $\Theta = \text{diag}(\theta) \in \mathbb{R}^{n \times n}$, $y_\theta = \Theta y$, and $\mathcal{L} = \Theta^{-1} Q \Theta^{-1}$. Because the elements of θ are non-negative, \mathcal{L} is non-negative definite.

The first part of the proof is to show that $\mathcal{L}\theta = \theta$. This is because $\Theta^{-2}Q$ is a Markov transition matrix. So,

$$\Theta^{-2}Q\mathbf{1}_n = \mathbf{1}_n \implies \Theta^{-1}Q\Theta^{-1}\Theta\mathbf{1}_n = \Theta\mathbf{1}_n$$

and this implies that $\mathcal{L}\theta = \theta$. So, by the Perron-Frobenius Theorem, θ is the leading eigenvector of \mathcal{L} with eigenvalue 1.

Let \mathcal{L} have eigenvectors and eigenvalues $(\phi_1, \lambda_1), \dots, (\phi_n, \lambda_n)$, where $\phi_1 = \theta/\|\theta\|_2$, $\lambda_1 = 1$ and $0 \leq \lambda_j \leq 1$ for $j \neq 1$. Then,

$$y^\top Q y = y_\theta^\top \mathcal{L} y_\theta = \sum_{\ell=1}^n \lambda_\ell \langle \phi_\ell, y_\theta \rangle^2.$$

Keeping only the first order term on the right-hand side, we have

$$y^\top Q y \geq \lambda_1 \langle \phi_1, y_\theta \rangle^2 = \frac{\langle d, \tilde{x}^2 \rangle^2}{\sum_i d_i}.$$

The desired result follows from the fact that $\sigma^2 = y^T Q y + y^T (Q - \text{diag}(Q)) y \geq y^T Q y$, since y and Q have non-negative entries. \square

Applying the bound in the lemma to the delocalization condition and rearranging gives the claim. \square

S1.2.3 Conditional CLT in the Bernoulli case

In Bernoulli graphs, the conditional mean of $\lambda_{\text{test}}(\tilde{x})$ is no longer $\lambda_{\varepsilon P}(\tilde{x})$ but takes a conditional form. Let $\Omega \in \{0, 1\}^{n \times n}$ be the adjacency matrix of an Erdős–Rényi graph with edge probability ε . Denote as \circ the element-wise matrix multiplication, $[P \circ \Omega]_{ij} := P_{ij} \Omega_{ij}$, and let J be the matrix filled with 1. We define the following random variables:

$$[\tilde{A}_{\text{test}}^\Omega]_{ij} \stackrel{\text{ind.}}{\sim} \text{Bernoulli}([P \circ \Omega]_{ij}),$$

$$[\tilde{A}^\Omega]_{ij} \stackrel{\text{ind.}}{\sim} \text{Bernoulli}([P \circ (J - \Omega)]_{ij}).$$

Observe that the random matrices \tilde{A}^Ω and $\tilde{A}_{\text{test}}^\Omega$ are conditionally independent given Ω . Let $\tilde{x} \in \mathbb{R}^n$ be any vector that only depends on \tilde{A}^Ω (e.g., an eigenvector). It follows that \tilde{x} and $\tilde{A}_{\text{test}}^\Omega$ are conditionally independent given Ω as well.

Given any unit vector $\tilde{x} \in \mathbb{R}^n$, we define the test statistic and sample total variance which will appear in the conditional CLT:

$$\lambda_{\text{test}}^\Omega(\tilde{x}) = \tilde{x}^T \tilde{A}_{\text{test}}^\Omega \tilde{x},$$

$$\hat{\sigma}_\Omega^2 = 2(\tilde{x}^2)^T \tilde{A}_{\text{test}}^\Omega \tilde{x}^2 - (\tilde{x}^2)^T \text{diag}(\tilde{A}_{\text{test}}^\Omega) \tilde{x}^2.$$

The conditional expectation of $\lambda_{\text{test}}^\Omega(\tilde{x})$ given Ω is $\lambda_{P \circ \Omega}(\tilde{x}) = \tilde{x}^T (P \circ \Omega) \tilde{x}$. Below, \tilde{x} and Ω are technically sequences depending on n , but we do not explicitly indicate the dependence on n for notational simplicity.

Proof of Theorem 3.2. We first show the CLT with the population variance σ_Ω^2 (in the

denominator),

$$\frac{\lambda_{\text{test}}^{\Omega}(\tilde{x}) - \lambda_{P \circ \Omega}(\tilde{x})}{\sigma_{\Omega}} \Rightarrow N(0, 1) \quad (\text{S10})$$

by verifying Lyapunov's condition. Then, we show the CLT holds when replacing population variance with the sample variance $\hat{\sigma}_{\Omega}$ via Slutsky's Lemma.

Since $\tilde{A}_{\text{test}}^{\Omega}$ is symmetric, only the triangular elements are independent. That is, for all $i \leq j$, $[\tilde{A}_{\text{test}}^{\Omega}]_{ij}$ are independent. For any $1 \leq i \leq j \leq n$, define random variables $X_{ij} = x_i x_j ([\tilde{A}_{\text{test}}^{\Omega}]_{ij} - [P \circ \Omega]_{ij})(2 - \mathbf{1}(i = j))$. Then, X_{ij} has conditional mean zero and conditional variance $\tilde{x}_i^2 \tilde{x}_j^2 [P \circ \Omega]_{ij} (1 - [P \circ \Omega]_{ij})(2 - \mathbf{1}(i = j))^2$. Furthermore, the numerator in Equation (S10) can be written as the sum of the X_{ij} 's, i.e., $\lambda_{\text{test}}^{\Omega}(\tilde{x}) - \lambda_{P \circ \Omega}(\tilde{x}) = \sum_{i \leq j} X_{ij}$. The sum of the X_{ij} 's conditional variances is equal to σ_{Ω}^2 by definition.

We verify the fourth moment Lyapunov's condition on the summation of X_{ij} for $i \leq j$ (see, e.g., Durrett [2019, Exercise 3.4.12])

$$\begin{aligned} \frac{\sum_{i \leq j} \mathbb{E}[|X_{ij}|^4 \mid \Omega]}{\sigma_{\Omega}^4} &= \frac{\sum_{i \leq j} \mathbb{E}\left[\left(x_i x_j ([\tilde{A}_{\text{test}}^{\Omega}]_{ij} - [P \circ \Omega]_{ij})(2 - \mathbf{1}(i = j))\right)^4 \mid \Omega\right]}{\sigma_{\Omega}^4} \\ &\stackrel{(i)}{\leq} \frac{\sum_{i \leq j} (\tilde{x}_i \tilde{x}_j)^4 [P \circ \Omega]_{ij} (1 - [P \circ \Omega]_{ij})(2 - \mathbf{1}(i = j))^4}{\sigma_{\Omega}^4} \\ &\leq \frac{4 \|\tilde{x}\|_{\infty}^4 \sum_{i \leq j} \tilde{x}_i^2 \tilde{x}_j^2 [P \circ \Omega]_{ij} (1 - [P \circ \Omega]_{ij})(2 - \mathbf{1}(i = j))^2}{\sigma_{\Omega}^4} \\ &= \frac{4 \|\tilde{x}\|_{\infty}^4}{\sigma_{\Omega}^2} \\ &\stackrel{(ii)}{=} o(1), \end{aligned}$$

where (i) comes from that the fourth central moment of a Bernoulli variable, $X \sim \text{Bernoulli}(p)$, satisfies $\mathbb{E}(X - p)^4 = p(1 - p)(p^3 + (1 - p)^3) \leq p(1 - p)$ and (ii) is due to the delocalization condition assumed. We also used that $\sigma_{\Omega} > 0$ eventually. This shows Equation (S10).

Via Slutsky's Lemma, we can multiply the ratio in Equation (S10) by any sequence that converges to one in probability and the result still holds. We then show that $\sigma_{\Omega}/\hat{\sigma}_{\Omega}$

converges to one in probability. Indeed, we have

$$\begin{aligned}
\text{Var} \left(\frac{\hat{\sigma}_\Omega^2}{\sigma_\Omega^2} \mid \Omega \right) &= \frac{\text{Var} \left(\sum_{i \leq j} \tilde{x}_i^2 \tilde{x}_j^2 [\tilde{A}_{\text{test}}^\Omega]_{ij} (2 - \mathbf{1}(i = j))^2 \mid \Omega \right)}{\sigma_\Omega^4} \\
&= \frac{\sum_{i \leq j} \tilde{x}_i^4 \tilde{x}_j^4 [P \circ \Omega]_{ij} (1 - [P \circ \Omega]_{ij}) (2 - \mathbf{1}(i = j))^4}{\sigma_\Omega^4} \\
&\leq \frac{4 \|\tilde{x}\|_\infty^4 \sum_{i \leq j} \tilde{x}_i^2 \tilde{x}_j^2 [P \circ \Omega]_{ij} (1 - [P \circ \Omega]_{ij}) (2 - \mathbf{1}(i = j))^2}{\sigma_\Omega^4} \\
&= \frac{4 \|\tilde{x}\|_\infty^4}{\sigma_\Omega^2} \\
&\stackrel{\text{(i)}}{=} o(1)
\end{aligned}$$

where (i) is the delocalization assumption. So, by Chebyshev's inequality, $\hat{\sigma}_\Omega^2/\sigma_\Omega^2$ converges in probability to its expectation given Ω . Note that

$$\begin{aligned}
\mathbb{E} \left(\frac{\hat{\sigma}_\Omega^2}{\sigma_\Omega^2} \mid \Omega \right) &= \frac{2(\tilde{x}^2)^\text{T} (P \circ \Omega) \tilde{x}^2 - (\tilde{x}^2)^\text{T} \text{diag}(P \circ \Omega) \tilde{x}^2}{2(\tilde{x}^2)^\text{T} (P \circ \Omega - P \circ P \circ \Omega) \tilde{x}^2 - (\tilde{x}^2)^\text{T} \text{diag}(P \circ \Omega - P \circ P \circ \Omega) \tilde{x}^2} \\
&\leq \frac{1}{1 - \max_{i,j} P_{ij}} \\
&\stackrel{\text{(i)}}{=} \frac{1}{1 - o(1)}
\end{aligned}$$

where (i) is due to the graph sparsity assumption. Similarly $\mathbb{E} \left(\frac{\hat{\sigma}_\Omega^2}{\sigma_\Omega^2} \mid \Omega \right) \geq 1$. Since taking the inverse and the square root is continuous transformation. So, the ratio $\sigma_\Omega/\hat{\sigma}_\Omega$ converges in probability to one, conditionally on Ω . \square

S1.3 Proof of consistency

This section details the proof of Theorem 4.1.

Notation We use the notation $[n]$ to refer to $\{1, 2, \dots, n\}$. For any real numbers $a, b \in \mathbb{R}$, we denote $a \vee b = \max\{a, b\}$ and $a \wedge b = \min\{a, b\}$. For non-negative a_n and b_n that depend on n , we write $a_n \lesssim b_n$ to mean $a_n \leq C b_n$ for some constant $C > 0$, and similarly for $a_n \gtrsim b_n$.

Also we write $a_n = O(b_n)$ to mean $a_n \leq Cb_n$ for some constant $C > 0$. The matrix spectral norm is $\|M\| = \max_{\|x\|_2=1} \|Mx\|_2$, the matrix max-norm is $\|M\|_{\max} = \max_{i,j} |M_{ij}|$, and the matrix $2 \rightarrow \infty$ norm is $\|M\|_{2,\infty} = \max_i \|M_{i,\cdot}\|_2$.

S1.3.1 Modified algorithm

Algorithm S1 is used in the consistency result.

Input: Adjacency matrix $A \in \mathbb{N}^{n \times n}$, edge splitting probability $\varepsilon \in (0, 1)$

Procedure $\text{EigCV}'(A, \varepsilon, k_{\max})$:

1. Obtain $\tilde{A}, \tilde{A}_{\text{test}} \leftarrow \text{ES}(A, \varepsilon)$ from splitting A and set $S = \emptyset$. // **Algorithm 1**

2. **for** $k = 2, \dots, k_{\max}$ **do**

a - compute $\tilde{\lambda}_{\text{test}}(\tilde{x}_k) = \tilde{x}_k^T \tilde{A}_{\text{test}} \tilde{x}_k$ and $\tilde{\sigma}_k = \sqrt{\frac{\varepsilon}{1-\varepsilon} (\tilde{x}_k^2)^T (2\tilde{A} - \text{diag}(\tilde{A})) \tilde{x}_k^2}$

b - if

$$\|\tilde{x}_k\|_{\infty}^2 \leq \min \left\{ \frac{\tilde{\sigma}_k^2}{\log^2 n}, \frac{\log n}{n} \right\},$$

add k to S and compute

$$T_k = \frac{\tilde{\lambda}_{\text{test}}(\tilde{x}_k)}{\tilde{\sigma}_k}.$$

Output: The graph dimensionality estimate: $\hat{K} = |\{T_k \geq \sqrt{n \log n} : k \in S\}|$.

Algorithm S1: Modified eigenvalue cross-validation

S1.3.2 Some concentration bounds

We will need several concentration bounds for Poisson random variables. We derive them from standard results.

We begin with a simple moment growth bound.

Lemma S1.2 (Poisson moment growth). *Let Z be a Poisson random variable with mean*

$\mu \leq 1$. There exists a universal constant $C > 0$ such that, for all integers $p \geq 2$,

$$\mathbb{E}[|Z - \mu|^p] \leq C\mu \frac{p!}{2} \left(\frac{e}{2}\right)^{p-2}.$$

Proof. We show that

$$\mathbb{E}[|Z - \mu|^p] \leq C' \mu \left(\frac{p}{2}\right)^p, \quad (\text{S11})$$

for some constant $C' > 0$. The claim then follows from Stirling's formula in the form

$$\sqrt{2\pi p} p^{p+1/2} e^{-p} \leq p!, \quad \forall p \geq 1.$$

By the definition of the Poisson distribution and using the fact that $0 \leq \mu \leq 1$ by assumption, we have

$$\begin{aligned} \mathbb{E}[|Z - \mu|^p] &= \sum_{z \geq 0} |z - \mu|^p e^{-\mu} \frac{\mu^z}{z!} \\ &= |\mu|^p e^{-\mu} + |1 - \mu|^p e^{-\mu} \mu + \sum_{z \geq 2} |z - \mu|^p e^{-\mu} \frac{\mu^z}{z!} \\ &\leq 2\mu + \mu^2 e \left\{ \sum_{z \geq 0} z^p \frac{e^{-1}}{z!} \right\}. \end{aligned}$$

The term in curly brackets on the last line is the p -th moment of a Poisson random variable with mean 1, which is $\leq C'' \left(\frac{p}{2}\right)^p$ for some constant $C'' > 0$ by Ahle [2021, Theorem 1]. Eq. (S11) follows. \square

The moment growth bound implies concentration for linear combinations of independent Poisson random variables.

Lemma S1.3 (General Bernstein for Poisson variables). *Let Z_1, \dots, Z_m be independent Poisson random variables with respective means $\mu_1, \dots, \mu_m \leq 1$. For any $\boldsymbol{\alpha} = (\alpha_1, \dots, \alpha_m) \in$*

\mathbb{R}^m and $t > 0$,

$$\mathbb{P} \left[\sum_{i=1}^m \alpha_i (Z_i - \mu_i) \geq t \right] \leq \exp \left(- \frac{t^2}{C' \mu_{\max} \|\boldsymbol{\alpha}\|_2^2 + C'' \|\boldsymbol{\alpha}\|_\infty t} \right),$$

where $\mu_{\max} = \max_i \mu_i$ and $C', C'' > 0$ are universal constants.

Proof. We use Boucheron et al. [2013, Corollary 2.11]. Observe that

$$\sum_{i=1}^m \mathbb{E}[\alpha_i (Z_i - \mu_i)^2] = \sum_{i=1}^m \alpha_i^2 \mu_i \leq \mu_{\max} \|\boldsymbol{\alpha}\|_2^2.$$

Moreover, by Lemma S1.2 and Stirling's formula,

$$\begin{aligned} \sum_{i=1}^m \mathbb{E}[\alpha_i^p (Z_i - \mu_i)_+^p] &\leq \sum_{i=1}^m \alpha_i^p C \mu_i \frac{p!}{2} \left(\frac{e}{2}\right)^{p-2} \\ &\leq C \mu_{\max} \|\boldsymbol{\alpha}\|_2^2 \frac{p!}{2} \left(\frac{e}{2} \|\boldsymbol{\alpha}\|_\infty\right)^{p-2} \\ &\leq \frac{p!}{2} v \left(\frac{e}{2} \|\boldsymbol{\alpha}\|_\infty\right)^{p-2}, \end{aligned}$$

where we define

$$v := \max\{1, C\} \mu_{\max} \|\boldsymbol{\alpha}\|_2^2.$$

The claim then follows from Boucheron et al. [2013, Corollary 2.11]. \square

The moment growth bound also implies spectral norm concentration.

Lemma S1.4 (Spectral norm of Poisson graph). *Suppose $B \in \mathbb{R}^{n \times n}$ is the adjacency matrix of a Poisson graph with mean matrix Q satisfying $Q_{ij} \leq 1$ for all i, j . Let $q_{\max} = \max_{ij} Q_{ij}$ and assume that $nq_{\max} \geq c_0 \log^{\xi_0} n$ for some $\xi_0 > 2$. Then, for any $\delta > 0$, there exists a constant $C''' > 0$ such that*

$$\|B - Q\| \leq C''' \sqrt{nq_{\max} \log n},$$

with probability at least $1 - n^{-\delta}$.

Proof. We use Tropp [2012, Theorem 6.2]. We first rewrite the matrix as a finite sum of independent symmetric random matrices

$$B - Q = \sum_{i=1}^n \sum_{j=i}^n (B_{ij} - Q_{ij}) E^{i,j},$$

where $E^{i,j} \in \mathbb{R}^{n \times n}$ with $E_{ij}^{i,j} = E_{ji}^{i,j} = 1$ and 0 elsewhere.

Observe that, for $i \neq j$,

$$(E^{i,j})^p = \begin{cases} E^{i,i} + E^{j,j} & \text{if } p = 2, 4, \dots \\ E^{i,j} & \text{if } p = 3, 5, \dots \end{cases}$$

while, if $i = j$,

$$(E^{i,i})^p = E^{i,i}, \quad p \geq 2.$$

Let $X^{i,j} := (B_{ij} - Q_{ij})E^{i,j}$. Then $\mathbb{E}X^{i,j} = 0$. Moreover, for $i \neq j$ and $p = 2, 4, \dots$, we have

$$\mathbb{E}(X^{i,j})^p = \mathbb{E}(B_{ij} - Q_{ij})^p (E^{i,i} + E^{j,j}) \preceq Cq_{\max} \frac{p!}{2} \left(\frac{e}{2}\right)^{p-2} (E^{i,i} + E^{j,j}),$$

by Lemma S1.2. Similarly, for $i \neq j$ and $p = 3, 5, \dots$,

$$\mathbb{E}(X^{i,j})^p = \mathbb{E}(B_{ij} - Q_{ij})^p E^{i,j} \preceq Cq_{\max} \frac{p!}{2} \left(\frac{e}{2}\right)^{p-2} (E^{i,i} + E^{j,j}),$$

where we used the fact that the matrix $\begin{pmatrix} 1 & \alpha \\ \alpha & 1 \end{pmatrix}$ has eigenvalues $1 + \alpha, 1 - \alpha \geq 0$ when $|\alpha| \leq 1$.

When $i = j$,

$$\mathbb{E}(X^{i,i})^p = \mathbb{E}(B_{ii} - Q_{ii})^p E^{i,i} \preceq Cq_{\max} \frac{p!}{2} \left(\frac{e}{2}\right)^{p-2} (2E^{i,i}).$$

Define

$$(\Sigma^2)^{i,j} := Cq_{\max} (E^{i,i} + E^{j,j}).$$

and

$$\sigma^2 = \left\| \sum_{i=1}^n \sum_{j=i}^n (\Sigma^2)^{i,j} \right\| = \left\| Cq_{\max} \sum_{i=1}^n \sum_{j=i}^n (E^{i,i} + E^{j,j}) \right\| \leq 2Cq_{\max}n,$$

where the inequality holds since $\sum_{i=1}^n \sum_{j=i}^n (E^{i,i} + E^{j,j})$ is a diagonal matrix with maximum entry $2n$. Then, by Tropp [2012, Theorem 6.2],

$$\begin{aligned} \mathbb{P} [\|B - Q\| \geq t] &= \mathbb{P} \left[\left\| \sum_{i=1}^n \sum_{j=i}^n X^{i,j} \right\| \geq t \right] \\ &\leq n \exp \left(\frac{-t^2/2}{\sigma^2 + (e/2)t} \right) \\ &\leq n \exp \left(\frac{-t^2/2}{2Cq_{\max}n + (e/2)t} \right). \end{aligned}$$

Taking $t = C''' \sqrt{nq_{\max} \log n}$ and using the fact that $nq_{\max} \geq c_0 \log^{\xi_0} n$, $\xi_0 > 2$, gives the result. \square

S1.3.3 Key properties of sample eigenvectors

Consider the adjacency matrix A of a Poisson graph satisfying Assumptions 1 and 2. Fixing $\varepsilon \in (0, 1)$, let \tilde{A} and \tilde{A}_{test} be as in Section 3. Let $P = \rho_n P^0 = \mathbb{E}A = \sum_{j=1}^K \lambda_j x_j^{\text{T}} x_j$ with $\lambda_1 \geq \lambda_2 \geq \dots \geq \lambda_K > 0$. Let $\{\tilde{x}_l\}_{l=1}^{k_{\max}}$ be the collection of eigenvectors associated with eigenvalues $\{\tilde{\lambda}_l\}_{l=1}^{k_{\max}}$ of \tilde{A} . Without loss of generality, we assume $\tilde{\lambda}_1 \geq \tilde{\lambda}_2 \geq \dots \geq \tilde{\lambda}_{k_{\max}}$. Define

$$\hat{U} = (\tilde{x}_1, \dots, \tilde{x}_K) \quad \text{and} \quad U = (x_1, \dots, x_K) \in \mathbb{R}^{n \times K}. \quad (\text{S12})$$

We will need the following event:

$$\mathcal{E}^0 = \left\{ \left\| \tilde{A} - (1 - \varepsilon)P \right\| \leq C''' \sqrt{n\rho_n \log n} \right\}.$$

Applying Lemma S1.4 with $B := \tilde{A}$ and $Q := (1 - \varepsilon)P$ shows that \mathcal{E}^0 holds with high probability.

Concentration of signal eigenspace First, we use a version of the Davis-Kahan theorem to show that the signal sample eigenvectors are close to the signal population eigenspace.

Lemma S1.5 (Signal eigenspace). *Under event \mathcal{E}^0 , there exists an orthonormal matrix $O \in \mathbb{R}^{K \times K}$ such that, for all $k \in [K]$,*

$$\|\tilde{y}_k - x_k\|_2 = O\left(\sqrt{\frac{\log n}{n\rho_n}}\right), \quad \|\tilde{x}_k - y_k\|_2 = O\left(\sqrt{\frac{\log n}{n\rho_n}}\right),$$

where

$$\tilde{y}_l = (\hat{U}O)_{\cdot l} = \left(\sum_{i=1}^K (\tilde{x}_i)_j O_{il}\right)_{j=1}^n, \quad y_l = (UO^T)_{\cdot l} = \left(\sum_{i=1}^K (x_i)_j O_{li}\right)_{j=1}^n.$$

Moreover, for all $k \in [K]$, $s \in [K]$, and $t \in [k_{\max}] \setminus [K]$,

$$\langle x_s, y_k \rangle = O_{ks}, \quad \langle \tilde{x}_t, \tilde{y}_k \rangle = 0.$$

Proof. We use the variant of the Davis-Kahan theorem in Yu et al. [2015, Theorem 2]. Under \mathcal{E}^0 , $\|\tilde{A} - (1 - \varepsilon)P\| = O(\sqrt{n\rho_n \log n})$. By Yu et al. [2015, Theorem 2], there exists an orthonormal matrix $O \in \mathbb{R}^{K \times K}$ such that, for all $l \in [K]$,

$$\|\tilde{y}_l - x_l\|_2 \leq \|\hat{U}O - U\|_F = O\left(\frac{\|\tilde{A} - (1 - \varepsilon)P\|}{\lambda_K}\right) = O\left(\sqrt{\frac{\log n}{n\rho_n}}\right),$$

and

$$\|\tilde{x}_l - y_l\|_2 \leq \|\hat{U} - UO^T\|_F = \|(\hat{U}O - U)O^T\|_F = \|\hat{U}O - U\|_F = O\left(\sqrt{\frac{\log n}{n\rho_n}}\right),$$

where we used $\lambda_K \geq \psi_1^{-1}\psi'_1 n\rho_n$, which holds under Assumption 1.

By the orthonormality of $\{x_l\}_l$ and $\{\tilde{x}_l\}_l$, we have for $s \in [K]$,

$$\langle x_s, y_k \rangle = \sum_{l=1}^n (x_s)_l \left(\sum_{i=1}^K (x_i)_l O_{ki} \right) = \sum_{i=1}^K \left(\sum_{l=1}^n (x_s)_l (x_i)_l \right) O_{ki} = O_{ks},$$

and for $t \in [k_{\max}] \setminus [K]$,

$$\langle \tilde{x}_t, \tilde{y}_k \rangle = \sum_{l=1}^n (\tilde{x}_t)_l \left(\sum_{i=1}^K (\tilde{x}_i)_l O_{ik} \right) = \sum_{i=1}^K O_{ik} \left(\sum_{l=1}^n (\tilde{x}_t)_l (\tilde{x}_i)_l \right) = \sum_{i=1}^K O_{ik} \mathbf{1}_{\{i=t\}} = 0.$$

□

Bounds on population quantities The previous lemma implies bounds on the population quantity of interest, $\lambda_P(\tilde{x}_l)$.

Lemma S1.6 (Bounding $\lambda_P(\tilde{x}_l)$). *Under event \mathcal{E}^0 ,*

$$\begin{aligned} \tilde{x}_l^\top P \tilde{x}_l &\gtrsim n\rho_n, & \forall l \in [K], \\ \tilde{x}_l^\top P \tilde{x}_l &\lesssim \log n, & \forall l \in [k_{\max}] \setminus [K]. \end{aligned}$$

Proof. For $s \in [K]$, expanding \tilde{x}_s over an orthonormal basis including $\{x_l\}_{l \in K}$, we get

$$\begin{aligned} \tilde{x}_s^\top P \tilde{x}_s &= \sum_{k=1}^K \lambda_k \langle \tilde{x}_s, x_k \rangle^2 \\ &= \sum_{k=1}^K \lambda_k \left[\langle x_k, y_s \rangle^2 - \langle x_k, y_s - \tilde{x}_s \rangle \langle x_k, \tilde{x}_s + y_s \rangle \right] \\ &\geq \sum_{k=1}^K \lambda_k O_{sk}^2 - \sum_{k=1}^K \lambda_k \|y_s - \tilde{x}_s\|_2 \|x_k\|_2^2 (\|\tilde{x}_s\|_2 + \|y_s\|_2) \end{aligned} \quad (\text{S13})$$

$$\begin{aligned} &\geq \psi_1^{-1} \psi'_1 n\rho_n - O \left(2K n\rho_n \sqrt{\frac{\log n}{n\rho_n}} \right) \\ &\gtrsim n\rho_n \end{aligned} \quad (\text{S14})$$

where inequality (S13) follows from Cauchy–Schwarz, the triangle inequality and $\langle x_k, y_s \rangle^2 =$

O_{sk} by Lemma S1.5. Inequality (S14) holds since $\sum_{k=1}^K O_{sk}^2 = 1$, $\psi_1^{-1}\psi_1' n\rho_n \leq \lambda_k \leq n\rho_n$ by Assumption 1, $\|\tilde{x}_s - y_s\|_2 = O\left(\sqrt{\frac{\log n}{n\rho_n}}\right)$ by Lemma S1.5 and $\|\tilde{x}_k\|_2 = \|x_k\|_2 = \|y_s\|_2 = 1$.

For $t \in [k_{\max}] \setminus [K]$,

$$\begin{aligned} \tilde{x}_t^\top P \tilde{x}_t &= \sum_{k=1}^K \lambda_k \langle \tilde{x}_t, x_k \rangle^2 \\ &= \sum_{k=1}^K \lambda_k \langle \tilde{x}_t, x_k - \tilde{y}_k + \tilde{y}_k \rangle^2 \\ &= \sum_{k=1}^K \lambda_k [\langle \tilde{x}_t, x_k - \tilde{y}_k \rangle + \langle \tilde{x}_t, \tilde{y}_k \rangle]^2 \\ &= \sum_{k=1}^K \lambda_k \langle \tilde{x}_t, x_k - \tilde{y}_k \rangle^2 \end{aligned} \tag{S15}$$

$$\leq K \lambda_1 \max_{k \in [K]} \|x_k - \tilde{y}_k\|_2^2 = O(\log n) \tag{S16}$$

where equality (S15) follows from $\langle \tilde{x}_t, \tilde{y}_k \rangle = 0$ by Lemma S1.5. Equation (S16) holds since $\|\tilde{y}_k - x_k\|_2 = O\left(\sqrt{\log n/n\rho_n}\right)$ by Lemma S1.5 and $\lambda_k \leq \lambda_1 \leq n\rho_n$ by Assumption 1. \square

Delocalization of signal eigenvectors To establish concentration of the estimate $\tilde{\lambda}_{\text{test}}(\tilde{x}_l)$ around $\varepsilon \lambda_P(\tilde{x}_l)$ for $l \in [K]$, we first need to show that \tilde{x}_l is delocalized. That result essentially follows from an entrywise version of Lemma S1.5 based on a technical result of Abbe et al. [2020].

Lemma S1.7 (Delocalization of signal sample eigenvectors). *There exist constants $\delta_1 > 0$, $C_1 > 0$ such that the event*

$$\mathcal{E}^1 = \left\{ \|\tilde{x}_l\|_\infty \leq C_1 \sqrt{\frac{\mu_0}{n}}, \forall l \in [K] \right\}$$

holds with probability at least $1 - 3n^{-\delta_1}$.

Proof. We use Abbe et al. [2020, Theorem 2.1] on \tilde{A} , which requires four conditions. We

check these conditions next. First, let $\tilde{A}^* = (1 - \varepsilon)P$, $\Delta^* = \lambda_K$,

$$\kappa = \frac{\lambda_1}{\lambda_K} \leq \psi_1, \quad (\text{S17})$$

where the inequality follows from Assumption 1,

$$\varphi(x) = \frac{1}{32\psi_1} \min\{\sqrt{nx}, 1\},$$

and

$$\gamma = C''' \psi_1 (\psi_1')^{-1} \sqrt{\frac{\log n}{n\rho_n}} \gtrsim \sqrt{\frac{\log n}{n^{1-\xi_1}}}, \quad (\text{S18})$$

where C''' is the constant in Lemma S1.4 and $\psi_1, \psi_1' > 0$, $\xi_1 \in (0, 1)$ are the constants in Assumption 1.

(A1) (*Incoherence*) By Abbe et al. [2020, Eq. (2.4)] and the remarks that follow it, the incoherence condition is satisfied provided

$$\mu(U) := \frac{n}{K} \|U\|_{2,\infty}^2 \leq \frac{n\gamma^2}{K\kappa^2}.$$

Under Assumption 2, $\mu(U) \leq \mu_0$ while (S18) implies $n\gamma^2 = \Omega(\log n)$ and (S17) implies $\kappa = O(1)$. Hence the condition is satisfied.

(A2) (*Row and columnwise independence*) By Lemma 3.1, \tilde{A} is the adjacency matrix of a Poisson graph with independent entries. In particular, $\{\tilde{A}_{ij} : i = m \text{ or } j = m\}$ are independent of $\{\tilde{A}_{ij} : i \neq m, j \neq m\}$.

(A3) (*Spectral norm concentration*) As observed previously, applying Lemma S1.4 with $B := \tilde{A}$, $Q := (1 - \varepsilon)P$ and $\delta > 0$ shows that the event

$$\mathcal{E}^0 = \left\{ \left\| \tilde{A} - (1 - \varepsilon)P \right\| \leq C''' \sqrt{n\rho_n \log n} \right\},$$

holds with probability $1 - n^{-\delta}$. Moreover, by the remark after Assumption 1,

$$\gamma\Delta^* = C''' \psi_1(\psi_1')^{-1} \sqrt{\frac{\log n}{n\rho_n}} \lambda_K \geq C''' \sqrt{n\rho_n \log n}.$$

Hence,

$$\mathbb{P} \left[\left\| \tilde{A} - \tilde{A}^* \right\| \leq \gamma\Delta^* \right] \geq 1 - n^{-\delta}.$$

Note further that, under Assumption 1, $\gamma = o(1)$, which implies

$$32\kappa \max\{\gamma, \varphi(\gamma)\} \leq 32\kappa \max\left\{\gamma, \frac{1}{32\psi_1}\right\} \leq 1,$$

for n large enough, as required in Abbe et al. [2020, Assumption (A3)], where we used (S17).

(A4) (*Row concentration*) As required in Abbe et al. [2020, Assumption (A4)], the function φ is continuous and non-decreasing on \mathbb{R}_+ with $\varphi(0) = 0$ and $\varphi(x)/x$ nonincreasing on \mathbb{R}_+ . Let $W \in \mathbb{R}^{n \times K}$. By standard norm bounds

$$\frac{1}{\sqrt{n}} \leq \frac{\|W\|_F}{\sqrt{n}\|W\|_{2,\infty}} \leq 1.$$

As a result, by definition of φ ,

$$\varphi\left(\frac{\|W\|_F}{\sqrt{n}\|W\|_{2,\infty}}\right) = \frac{1}{32\psi_1}.$$

Let

$$g = \Delta^* \|W\|_{2,\infty} \varphi\left(\frac{\|W\|_F}{\sqrt{n}\|W\|_{2,\infty}}\right) = \frac{1}{32\psi_1} \lambda_K \|W\|_{2,\infty}.$$

Fix $m \in [n]$ and $r \in [K]$. Applying Lemma S1.3 on \tilde{A}_m . with $\max_{ij} \mathbb{E}\tilde{A}_{ij} \leq (1 - \varepsilon)\rho_n$,

there exist $c_2 > 0$, $c'_2 > 1$ such that

$$\begin{aligned}
& \mathbb{P} \left(\left| \sum_{i \in [n]} (\tilde{A}_{mi} - \tilde{Q}_{mi}) W_{ir} \right| \geq g/\sqrt{K} \right) \\
& \leq 2 \exp \left(- \frac{g^2/K}{C'(1-\varepsilon)\rho_n \|W_{\cdot r}\|_2^2 + C'' \|W_{\cdot r}\|_\infty g/\sqrt{K}} \right) \\
& = 2 \exp \left(- \frac{\lambda_K^2 \|W\|_{2,\infty}^2}{32^2 \psi_1^2 K C'(1-\varepsilon)\rho_n \|W_{\cdot r}\|_2^2 + 32 \psi_1 \sqrt{K} C'' \|W_{\cdot r}\|_\infty \lambda_K \|W\|_{2,\infty}} \right) \\
& \leq 2 \exp \left(- \frac{\lambda_K^2}{32^2 \psi_1^2 K C'(1-\varepsilon)n\rho_n + 32 \psi_1 \sqrt{K} C'' \lambda_K} \right) \\
& \leq 2 \exp(-c_2 n \rho_n) \\
& \leq n^{-c'_2},
\end{aligned}$$

where C' and C'' are the constants in Lemma S1.3 and we used again that, by the remark after Assumption 1, $\lambda_K \geq \psi_1^{-1} \psi'_1 n \rho_n$. In the final inequality, we use that $n \rho_n \geq c_0 \log^{\xi_0} n$, $\xi_0 > 2$ under Assumption 1. Since

$$\left\| (\tilde{A} - \tilde{Q})_{m \cdot} W \right\|_2 \leq \sqrt{K} \sup_r \left| \sum_{i \in [n]} (\tilde{A}_{mi} - \tilde{Q}_{mi}) W_{ir} \right|,$$

a union bound over r implies

$$\mathbb{P} \left[\left\| (\tilde{A} - \tilde{Q})_{m \cdot} W \right\|_2 \leq g \right] \geq 1 - K n^{-c'_2}.$$

Recall the definition of \hat{U} and U from (S12). Applying Abbe et al. [2020, Theorem 2.1] and using Abbe et al. [2020, Eq. (2.4)] again, there exists $\tilde{C} > 0$ such that

$$\begin{aligned}
\max_{l \in [K]} \|\tilde{x}_l\|_\infty & \leq \left\| \hat{U} \right\|_{2,\infty} \\
& \leq \tilde{C} (2\kappa + \varphi(1)) \|U\|_{2,\infty} \\
& \leq \tilde{C} \left(2\psi_1 + \frac{1}{32\psi_1} \right) \sqrt{K} \sqrt{\frac{\mu_0}{n}},
\end{aligned}$$

with probability $1 - n^{-\delta} - 2n^{-(c'_2-1)}$, where we used Assumption 2 on the last line. Taking $C_1 = \tilde{C}(2\psi_1 + \frac{1}{32\psi_1})\sqrt{K}$ and $\delta_1 = \min\{\delta, c'_2 - 1\} > 0$ gives the claim. \square

Concentration of quadratic forms We bound the variance estimate for the signal eigenvectors.

Lemma S1.8 (Bound on the variance estimate). *Under event $\mathcal{E}^0 \cap \mathcal{E}^1$, for all $l \in [K]$,*

$$\tilde{\sigma}_l^2 := \frac{\varepsilon}{1-\varepsilon} (\tilde{x}_l^2)^\top \left(2\tilde{A} - \text{diag}(\tilde{A}) \right) \tilde{x}_l^2 = \Theta(\rho_n).$$

Proof. Let $\tilde{Q} = (1-\varepsilon)P$. We first show $(\tilde{x}_l^2)^\top \tilde{A} \tilde{x}_l^2$ can be controlled via $(\tilde{x}_l^2)^\top \tilde{Q} \tilde{x}_l^2$. Indeed observe that for each $l \in [K]$

$$\begin{aligned} \left| (\tilde{x}_l^2)^\top \tilde{A} \tilde{x}_l^2 - (\tilde{x}_l^2)^\top \tilde{Q} \tilde{x}_l^2 \right| &= |(\tilde{x}_l^2)^\top (\tilde{A} - \tilde{Q}) \tilde{x}_l^2| \\ &\leq \left\| \tilde{A} - \tilde{Q} \right\| \|\tilde{x}_l^2\|_2^2 \\ &\leq \left\| \tilde{A} - \tilde{Q} \right\| \|\tilde{x}_l\|_\infty^2 \|\tilde{x}_l\|_2^2 \\ &= O\left(\sqrt{n\rho_n \log n} \cdot \frac{1}{n} \right) \\ &= O\left(\sqrt{\frac{\rho_n \log n}{n}} \right) \end{aligned}$$

where we used that $\left\| \tilde{A} - \tilde{Q} \right\| = O(\sqrt{n\rho_n \log n})$ under event \mathcal{E}^0 and $\|\tilde{x}_l^2\|_\infty = \|\tilde{x}_l\|_\infty^2 = O(\frac{1}{n})$ under \mathcal{E}^1 . Moreover, observe that $\sqrt{\rho_n \log n/n} \ll \rho_n$ since $n\rho_n \geq c_0 \log^{50} n$ under Assumption 1. So

$$\left| (\tilde{x}_l^2)^\top \tilde{A} \tilde{x}_l^2 - (\tilde{x}_l^2)^\top \tilde{Q} \tilde{x}_l^2 \right| \ll \rho_n. \tag{S19}$$

To get an upper bound on $\tilde{\sigma}_l^2$, note that

$$\begin{aligned}
(\tilde{x}_l^2)^\top P \tilde{x}_l^2 &\leq \lambda_1 \|\tilde{x}_l^2\|_2^2 \\
&\leq \lambda_1 \cdot \|\tilde{x}_l\|_\infty^2 \cdot \|\tilde{x}_l\|_2^2 \\
&= O\left(n\rho_n \cdot \frac{1}{n} \cdot 1\right) \\
&= O(\rho_n),
\end{aligned}$$

where we used $\lambda_1 \leq n\rho_n$ by Assumption 1. Hence, we get

$$\begin{aligned}
\tilde{\sigma}_l^2 &= \frac{\varepsilon}{1-\varepsilon} \left[2(\tilde{x}_l^2)^\top \tilde{A} \tilde{x}_l^2 - (\tilde{x}_l^2)^\top \text{diag}(\tilde{A}) \tilde{x}_l^2 \right] \\
&\leq \frac{2\varepsilon}{1-\varepsilon} (\tilde{x}_l^2)^\top \tilde{A} \tilde{x}_l^2 \\
&\leq \frac{2\varepsilon}{1-\varepsilon} |(\tilde{x}_l^2)^\top \tilde{A} \tilde{x}_l^2 - (\tilde{x}_l^2)^\top \tilde{Q} \tilde{x}_l^2| + \frac{2\varepsilon}{1-\varepsilon} (\tilde{x}_l^2)^\top \tilde{Q} \tilde{x}_l^2 \\
&\leq \frac{2\varepsilon}{1-\varepsilon} |(\tilde{x}_l^2)^\top \tilde{A} \tilde{x}_l^2 - (\tilde{x}_l^2)^\top \tilde{Q} \tilde{x}_l^2| + 2\varepsilon (\tilde{x}_l^2)^\top P \tilde{x}_l^2 \\
&= O(\rho_n),
\end{aligned}$$

by (S19).

In the other direction, by Cauchy-Schwarz,

$$(\tilde{x}_l^2)^\top P \tilde{x}_l^2 \geq \frac{(\tilde{x}_l^\top P \tilde{x}_l)^2}{\sum_{ij} P_{ij}} \gtrsim \frac{(n\rho_n)^2}{n^2\rho_n} \gtrsim \rho_n,$$

where the middle inequality follows from Lemma S1.6. Combining with (S19), we have

$$\begin{aligned}
\tilde{\sigma}_l^2 &= \frac{\varepsilon}{1-\varepsilon} \left[(\tilde{x}_l^2)^\top \tilde{A} \tilde{x}_l^2 + (\tilde{x}_l^2)^\top \left(\tilde{A} - \text{diag}(\tilde{A}) \right) \tilde{x}_l^2 \right] \\
&\geq \frac{\varepsilon}{1-\varepsilon} (\tilde{x}_l^2)^\top \tilde{A} \tilde{x}_l^2 \\
&\geq \frac{\varepsilon}{1-\varepsilon} (\tilde{x}_l^2)^\top \tilde{Q} \tilde{x}_l^2 - \frac{\varepsilon}{1-\varepsilon} \left| (\tilde{x}_l^2)^\top \tilde{A} \tilde{x}_l^2 - (\tilde{x}_l^2)^\top \tilde{Q} \tilde{x}_l^2 \right| \\
&= \varepsilon (\tilde{x}_l^2)^\top P \tilde{x}_l^2 - \frac{\varepsilon}{1-\varepsilon} \left| (\tilde{x}_l^2)^\top \tilde{A} \tilde{x}_l^2 - (\tilde{x}_l^2)^\top \tilde{Q} \tilde{x}_l^2 \right| \\
&\gtrsim \rho_n.
\end{aligned}$$

That concludes the proof. \square

Finally, before moving on to the proof of the main theorem, we show next that $\tilde{\lambda}_{\text{test}}(\tilde{x}_l)$ is concentrated around $\varepsilon\lambda_P(\tilde{x}_l)$.

Lemma S1.9 (Concentration of $\tilde{\lambda}_{\text{test}}(x)$). *Let $x \in \mathbb{R}^n$ be a unit vector such that*

$$\|x\|_\infty^2 \leq \frac{\log n}{n}, \quad (\text{S20})$$

then there exists $\delta_2 > 1$ such that

$$\mathbb{P} \left[\left| \sum_{i,j} x_i x_j (\tilde{A}_{\text{test}} - \varepsilon P)_{ij} \right| \leq \sqrt{\rho_n \log n} \right] \geq 1 - n^{-\delta_2}.$$

Proof. We use Lemma S1.3. From $\|x\|_2 = 1$, we get

$$\begin{aligned} & \mathbb{P} \left[\left| \sum_{i,j} x_i x_j (\tilde{A}_{\text{test}} - \varepsilon P)_{ij} \right| \geq \sqrt{\rho_n \log n} \right] \\ & \leq 2 \exp \left(- \frac{(\sqrt{\rho_n \log n})^2 / 2}{C' \varepsilon \rho_n \sum_{i,j} (x_i x_j)^2 + C'' \max_{i,j} |x_i x_j| \sqrt{\rho_n \log n}} \right) \\ & \leq 2 \exp \left(- \frac{\rho_n \log n / 2}{C' \varepsilon \rho_n + C'' \|x\|_\infty^2 \sqrt{\rho_n \log n}} \right). \end{aligned}$$

By Assumption 1, $\rho_n \gg \frac{\log n}{n}$ while $\sqrt{\rho_n \log n} = o(1)$. By (S20), the denominator on the last line is $\lesssim \rho_n$ and the claim follows. \square

S1.3.4 Proof of Theorem 4.1

Now, we are ready to prove Theorem 4.1.

Proof of Theorem 4.1. By Lemmas S1.4 and S1.7, the event $\mathcal{E}^0 \cap \mathcal{E}^1$ holds with probability $1 - 4n^{-\delta_1}$. Under $\mathcal{E}^0 \cap \mathcal{E}^1$, which depends only on \tilde{A} , the claims in Lemmas S1.5, S1.6 and S1.8 also hold. For the rest of the proof, we condition on $\mathcal{E}^0 \cap \mathcal{E}^1$ and use the fact that \tilde{A}_{test} is independent of \tilde{A} by Lemma 3.1.

Let $\tilde{x}_l, l \in [k_{\max}]$, be the top k_{\max} unit eigenvectors of \tilde{A} and let

$$\tilde{\sigma}_l^2 = \frac{\varepsilon}{1-\varepsilon} (\tilde{x}_l^2)^\top \left(2\tilde{A} - \text{diag}(\tilde{A}) \right) \tilde{x}_l^2.$$

Define

$$S = \left\{ l \in [k_{\max}] : \|\tilde{x}_l\|_\infty^2 \leq \min \left\{ \frac{\tilde{\sigma}_l^2}{\log^2 n}, \frac{\log n}{n} \right\} \right\},$$

to be the subset of $[k_{\max}]$ corresponding to sufficiently delocalized eigenvectors. Recall that the test statistic associated to \tilde{x}_l is

$$T_l = \frac{\tilde{x}_l^\top \tilde{A}_{\text{test}} \tilde{x}_l}{\tilde{\sigma}_l}.$$

We say that l is rejected if

$$l \in S \quad \text{and} \quad |T_l| \geq \sqrt{n \log n} =: \tau_n.$$

No under-estimation We show that the test statistic associated with the K leading eigenvectors of \tilde{A} will reject the null hypothesis with high probability, that is,

- $[K] \subset S$; and
- $|T_l| \geq \tau_n, \forall l \in [K]$.

Fix $s \in [K]$. First, we check that $s \in S$. Under \mathcal{E}^1 , $\|\tilde{x}_s^2\|_\infty = O(1/n) \ll \log n/n$. We need to check that $\|\tilde{x}_s^2\|_\infty \leq \tilde{\sigma}_s^2 / \log^2 n$, for n sufficiently large. This follows from the fact that $\tilde{\sigma}_s^2 = \Theta(\rho_n)$ by Lemma S1.8 and $\rho_n \geq c_0 n^{-1} \log^{\xi_0} n$ with $\xi_0 > 2$ under Assumption 1.

Next, we bound $|T_s|$ from below. We have, with probability $1 - n^{-\delta_2}$, where $\delta_2 > 1$ is

the constant in Lemma S1.9,

$$\begin{aligned}
|T_s| &= \left| \frac{\tilde{x}_s^\top \tilde{A}_{\text{test}} \tilde{x}_s}{\tilde{\sigma}_s} \right| \\
&\geq \frac{\varepsilon |\tilde{x}_s^\top P \tilde{x}_s| - |\tilde{x}_s^\top (\tilde{A}_{\text{test}} - \varepsilon P) \tilde{x}_s|}{\tilde{\sigma}_s} \\
&\gtrsim \frac{\varepsilon n \rho_n - \sqrt{\rho_n \log n}}{\sqrt{\rho_n}} \\
&\gtrsim n \sqrt{\rho_n} \\
&\gg \sqrt{n \log n}, \tag{S21}
\end{aligned}$$

where the dominating term is controlled through $|\tilde{x}_s^\top P \tilde{x}_s| \gtrsim n \rho_n \gg \log n$ by Lemma S1.6, the term $|\tilde{x}_s^\top (\tilde{A}_{\text{test}} - \varepsilon P) \tilde{x}_s|$ is bounded above by $\sqrt{\rho_n \log n} \ll \log n$ from Lemma S1.9 and the denominator satisfies $\tilde{\sigma}_s^2 = \Theta(\rho_n)$ by Lemma S1.8. The final bound follows from Assumption 1. By a union bound, (S21) holds simultaneously for $s \in [K]$ with probability $1 - K n^{-\delta_2}$.

No over-estimation Then, we show that the noise eigenvectors of \tilde{A} will either be too localized or the test statistic associated with them will fail to reject the null hypothesis. In other words, we show that for any $s \in S \setminus [K]$, it holds that $|T_s| < \tau_n$ with high probability.

Let $t \in S \setminus [K]$. We bound $|T_t|$ from above as follows

$$\begin{aligned}
|T_t| &= \left| \frac{\tilde{x}_t^\top \tilde{A}_{\text{test}} \tilde{x}_t}{\tilde{\sigma}_t} \right| \\
&\leq \frac{\varepsilon |\tilde{x}_t^\top P \tilde{x}_t| + |\tilde{x}_t^\top (\tilde{A}_{\text{test}} - \varepsilon P) \tilde{x}_t|}{\tilde{\sigma}_t} \tag{S22}
\end{aligned}$$

$$\begin{aligned}
&= O\left(\sqrt{\frac{n}{\log^2 n}} \cdot (\log n + \sqrt{\rho_n \log n})\right) \\
&= O(\sqrt{n}). \tag{S23}
\end{aligned}$$

The first term in the numerator of (S22) satisfies $|\tilde{x}_t^\top P \tilde{x}_t| = O(\log n)$ by Lemma S1.6

while the term $|\tilde{x}_t^\top(\tilde{A}_{\text{test}} - \varepsilon P)\tilde{x}_t|$ in (S22) is bounded above by $\sqrt{\rho_n \log n} \ll \log n$ from Lemma S1.9. For the denominator $\tilde{\sigma}_t$, $t \in S$ implies that $\|\tilde{x}_t^2\|_\infty \leq \tilde{\sigma}_t^2 / \log^2 n$, thus

$$\tilde{\sigma}_t^2 \geq \log^2 n \cdot \|\tilde{x}_t^2\|_\infty \geq \frac{\log^2 n}{n} \cdot n \|\tilde{x}_t^2\|_\infty \geq \frac{\log^2 n}{n} \cdot \|\tilde{x}_t\|_2^2 = \frac{\log^2 n}{n}.$$

By a union bound, (S23) holds simultaneously for $t \in S \setminus [K]$ with probability at least $1 - n^{-\delta_2+1}$.

Consistency Therefore, it follows that the algorithm outputs $\hat{K} = K$ with probability tending to 1. \square

Remark S1.1. *A similar result can be obtained in the Bernoulli case. As we explained in the context of the CLT, one loses the independence of \tilde{A}_{test} and \tilde{A} which is used to apply Lemma S1.9 in the proof of the theorem. But one can instead condition on which pairs of vertices $\Omega \subseteq \{(i, j) : 1 \leq i < j \leq n\}$ are set aside for the test graph – before generating \tilde{A} and \tilde{A}_{test} . In that case, the two graphs are conditionally independent. The key difference is that εP is replaced with the conditional version $\mathcal{P}_\Omega P$ in Lemma S1.9, where recall that $\mathcal{P}_\Omega P \in \mathbb{R}^{n \times n}$ is the matrix with entries*

$$(\mathcal{P}_\Omega P)_{ij} := P_{ij} \mathbf{1}\{(i, j) \in \Omega \text{ or } (j, i) \in \Omega\}.$$

One can then use Lemma 2 in the supplementary materials of [Li et al., 2020] to show that the two mean quantities are close. We omit the details.

S2 Details on motivating examples

In the introduction, the simulated graph comes from a Degree-Corrected Stochastic Block-model (DCSBM). See Section 5.1 for a description of this model and its parameters. In Figures 1 and 2, the DCSBM has $k = 128$ blocks. The 2,560 nodes are randomly assigned to the 128 blocks with uniform probabilities. On average, each block contains 20 nodes.

The smallest block has 10 nodes and the largest block has 32. The degree parameters θ_i are distributed as $\text{Exponential}(\lambda = 1)$ and the B matrix is hierarchically structured. In order to specify the elements of B , let \mathbb{T} be a complete binary tree with 7 generations (i.e., $2^7 = 128$ leaves). Each leaf node is assigned to one of the $k = 128$ blocks. Define $u \wedge v \in \mathbb{T}$ as the most recent common ancestor of u and v (i.e., the node closest to the root along the shortest path between u and v). Define $g(u, v)$ as the distance in \mathbb{T} from the root to $u \wedge v$. So, if the shortest path between u and v passes through the root, then $g(u, v) = 0$. Moreover, $g(u, u) = 7$ for all leaf nodes u . Set $B_{u,v} = p2^{g(u,v)}$, where $p = .0008$ is chosen so that the average expected degree of the nodes is equal to 20.

The citation graph was originally constructed and studied in Rohe and Zeng [2020]. There are roughly 220 million academic papers in the dataset. Citations from one paper to another were converted to citations between the journals that published the papers. If there were more than 5 citations from journal i to journal j using a 5% sample of all edges, then A_{ij} is set to one. Otherwise, A_{ij} is zero. For simplicity, the graph was symmetrized by setting $A_{ij} = 1$ if $A_{ji} = 1$. In this example, $\varepsilon = .05$ and for illustration, the data was divided only one time.

The illustration in Figures 1 and 2 splits the edges ten separate times, each with probability $\varepsilon = .1$, and averages the results over those ten folds.

S3 Poisson vs. Bernoulli

The Poisson model has previously been used to study statistical inference with random graphs [Karrer and Newman, 2011, Flynn et al., 2020, Crane and Dempsey, 2018, Cai et al., 2016, Zhou and Amini, 2020]). In the sparse graph setting, these models produce very similar graphs (e.g. Theorem 7 in Rohe et al. [2018]). Moreover, under the Poisson model, the edges are exchangeable [Cai et al., 2016, Crane and Dempsey, 2018, Rohe et al., 2018].

This section shows that **EigCV** continues to perform well in settings where the elements

of A are Bernoulli random variables. The technical results and derivations in this paper do not directly apply to this setting. The key difficulty comes from the edge splitting. Under the Bernoulli model, $A_{ij} \in \{0, 1\}$. So, it is not possible for both \tilde{A} and \tilde{A}_{test} to get the edge i, j . This creates *negative* dependence. Because the fitting and test graph are dependent, a central limit theorem akin to Theorem 3.1 becomes more difficult (Theorem 3.2). Nevertheless, a theorem akin to Theorem 4.1 still holds with minor changes to the conditions.

This simulation shows that the negative dependence created from Bernoulli edges makes the testing procedure more conservative. That is, when we are testing

$$H_0 : \mathbb{E}(\lambda_{\text{test}}(\tilde{x}_\ell)) = 0$$

for $\ell > k$, the $\alpha = .05$ test rejects with probability less than .05. This type of miscalibration is traditionally considered acceptable.

This section simulates from a $k = 2$ Stochastic Blockmodel and examines the distribution of T_3 and T_4 , under both the Bernoulli and Poisson models for edges. In all of these simulations, there are $n = 2000$ nodes. Each node is randomly assigned to either block 1 or 2 with equal probabilities. Let i and j be any two nodes in the same block and u and v be any two nodes in different blocks. Across simulation settings, $P_{ij}/P_{u,v} = 2.5$. While keeping this ratio constant, the values in P increase to make the expected degree of the graph go from 3.5 to 105, by increments of 3.5. In the Poisson model, $A_{ij} \sim \text{Poisson}(P_{ij})$ and in the Bernoulli model, $A_{ij} \sim \text{Bernoulli}(P_{ij})$. We compute T_3 and T_4 in EigCV (Algorithm 2) with edge split probability $\varepsilon = .05$ and folds = 1. Supplementary Section S3.2 gives the identical simulation, but for folds = 10.

We use the one-sided rejection region $T_\ell > 1.65$. If $T_\ell \sim N(0, 1)$, then this has level $\alpha = .05$. We refer to the simulated probability that $T_\ell > 1.65$ as the rejection probability. Figure S1 estimates the rejection probability in two ways. First, each dot gives the proportion of

1000 replicates in which $T_\ell > 1.65$. Second, the line gives the values

$$\hat{\alpha} = 1 - \Phi((1.65 - \bar{T}_\ell)/SD(T_\ell)), \tag{S24}$$

where Φ is the cumulative distribution function (CDF) of the standard normal, \bar{T}_ℓ is the average value of T_ℓ over the 1000 replicates, and $SD(T_\ell)$ is the standard deviation of these 1000 replicates. This is an estimate of the rejection probability, under the assumption that T_ℓ is normally distributed.

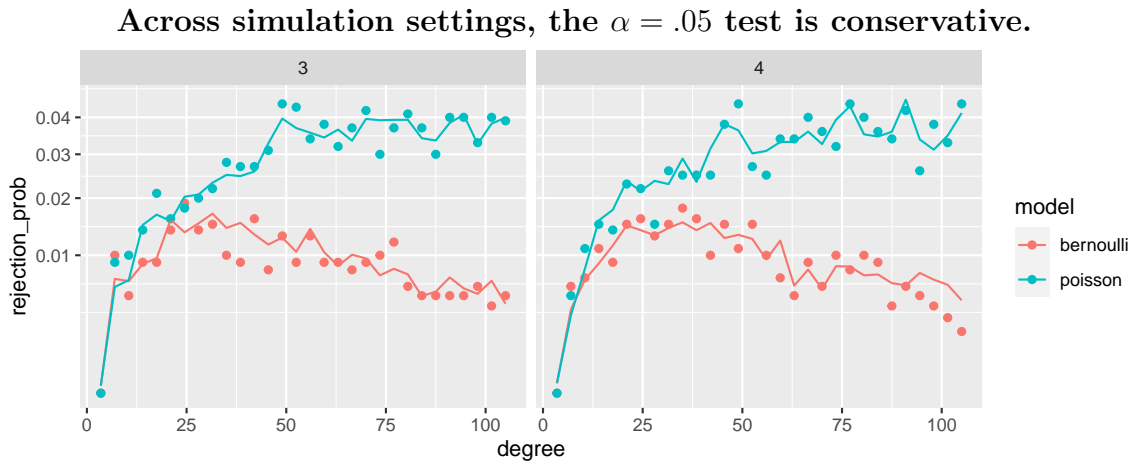


Figure S1: The left panel gives results for T_3 and the right panel gives results for T_4 . Each point corresponds to the proportion of 1000 replicates that the test statistic was greater than 1.65. The line is a smoothed version of $\hat{\alpha}$.

Under the simulation settings described above, Figure S1 shows four things.

1. The points and lines are below .05. So, the proposed test is conservative.
2. On the left side of both panels, the points and lines are well below .05. So, the proposed test is particularly conservative for very sparse graphs. Note that the bottom left point in both figures is over-plotted with two points. This is because none of the 4000 tests in the lowest degree graphs were rejected. The corresponding $\hat{\alpha}$'s are on the order 1/20,000.

3. On the right side of both panels, the red line decreases. So, for Bernoulli graphs, the test is increasingly conservative for denser graphs.
4. The points are scattered around their respective lines, which suggests that the normal distribution provides a reasonable approximation for the right tail of the distribution (but T_ℓ does not have expectation zero and variance one).

The test is increasingly conservative for dense Bernoulli graphs. In particular, the line giving the normal approximation $\hat{\alpha}$ is decreasing. So, either $\mathbb{E}(T_3) < 0$ or $\text{Var}(T_3) < 1$ or both (and similarly for T_4). The next figure, Figure S2, shows that the expectation of T_3 and T_4 decreases away from zero for dense Bernoulli graphs.

Under the Bernoulli model, for $\ell > k$, the negative dependence makes the expectation of T_ℓ decrease away from zero as the graph becomes more dense.

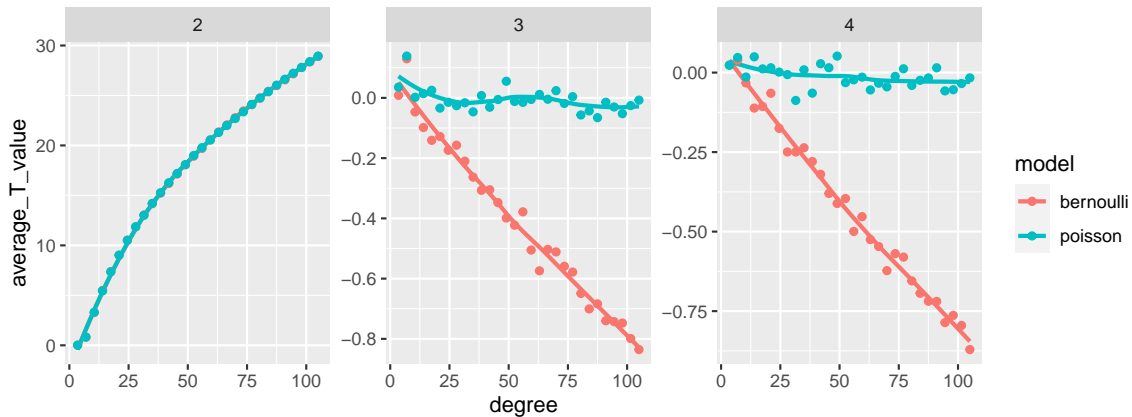


Figure S2: Each dot gives the average value of T_ℓ over 1000 replicates; T_2 on the left, T_3 in the middle, and T_4 on the right. The previous figure, Figure S1, shows that as the Bernoulli graph becomes denser, T_3 and T_4 are less likely to exceed 1.65. This figure shows that this is because their expectation decreases away from zero.

The expected values of T_3 and T_4 decrease due to the negative dependence between \tilde{A} and \tilde{A}_{test} under the Bernoulli model, as anticipated by the conditional nature of the CLT in Theorem 3.2. That is, if an edge appears in \tilde{A} , then it cannot appear in \tilde{A}_{test} , and vice versa. Figure S2 shows that $\tilde{x}_\ell^T \tilde{A} \tilde{x}_\ell$ and $\tilde{x}_\ell^T \tilde{A}_{\text{test}} \tilde{x}_\ell$ are negatively correlated when (1) the edges are Bernoulli, (2) the graph is dense, (3) and $\ell > k$. In the two-block Stochastic

Blockmodel, this negative dependence does not shift the expectation of T_2 , even for dense Bernoulli graphs (see also Figure S3 below). The fact that \tilde{x}_ℓ displays negative correlation, but only for $\ell > k$, is particularly interesting. Here is one interpretation: because these eigenvectors do not estimate signal, they only find noise in \tilde{A} . Then, that noise disappears in \tilde{A}_{test} due to the negative dependence.

On the very left of both panels in Figure S1, the expected degree is 3.5. In this very sparse regime, which is below the weak recovery threshold [Mossel et al., 2015] (see also Abbe [2018]), the tests are conservative for both Bernoulli and Poisson graphs. In this very sparse regime, the eigenvectors \tilde{x}_ℓ often localize on a few nodes that have a large degree simply due to chance. When this happens, $(\tilde{x}_\ell^2)^T A \tilde{x}_\ell^2$ over-estimates the population quantity $(\tilde{x}_\ell^2)^T \mathbb{E}(A) \tilde{x}_\ell^2$. This causes $\tilde{\sigma}_\ell$ in the denominator of T_ℓ to be large, thus making the standard deviation of T_ℓ small and the test statistic less likely to exceed 1.65. Figure S4 below displays the standard deviation of the test statistics. It is comforting that the test is conservative in such scenarios because these localized eigenvectors \tilde{x} are often particularly troubling artifacts of noise. For example, the consistency result in Section 4.2 requires an additional step to **EigCV** that discards localized eigenvectors. The current simulation suggests that the additional step is a technical requirement. For this reason, we do not include the additional step in **EigCV**.

Supplementary Section S3.2 repeats these figures with $\text{folds} = 10$. Increasing the number of folds makes the T_3 and T_4 even more conservative, while making T_2 more powerful. This happens because the variation in T_ℓ comes from both the original data A and the edge splitting. By increasing the number of folds, the second source of variation diminishes while not disrupting the expectation of T_ℓ .

S3.1 Two clarifying figures for $\text{folds} = 1$

The average value of T_3 and T_4 are different under the Poisson and Bernoulli models (see Figure S2 in Section S3). To further illustrate this difference and to show that T_2 does not have the same property, Figure S3 subtracts the average value of the test statistic *under the*

Bernoulli model from the corresponding average under the Poisson model. The difference appears for T_3 and T_4 , but not for T_2 . This shows that $\tilde{x}_\ell^T \tilde{A} \tilde{x}_\ell$ and $\tilde{x}_\ell^T \tilde{A}_{\text{test}} \tilde{x}_\ell$ are negatively correlated when (1) the edges are Bernoulli, (2) the graph is dense, (3) and $\ell > k$. In the two-block Stochastic Blockmodel, this negative dependence does not shift the expectation of T_2 , even for dense Bernoulli graphs.

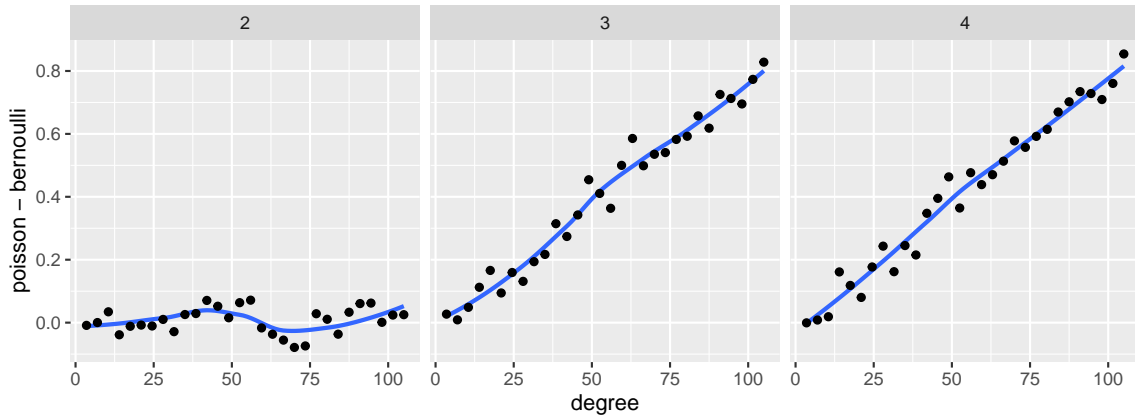


Figure S3: Each panel gives the difference between the Poisson and Bernoulli results from Figure S2. In this simulation model, there are $k = 2$ blocks in the Stochastic Blockmodel. Taken together, this suggests that the negative dependence in Bernoulli graphs between the fitting and testing adjacency matrices diminishes the expected value of T_ℓ when $\ell > k$ and the graph is more dense. However, the negative dependence does not appear to diminish the expected value of T_2 . When a test is conservative under the null, one typically suffers a reduced power under the alternative. However, this result suggests that the negative dependence require us to pay this price. The Bernoulli model makes T_3 conservative, without making T_2 less powerful.

Figure S4 displays the standard deviation for the test statistics T_2, T_3, T_4 over the 1000 replicates in the simulation. This figure is repeated with folds = 10 in Figure S6.

S3.2 Increasing the number of folds in the Bernoulli vs. Poisson comparison

Figure S5 repeats Figure S1, but with folds = 10 instead of 1. It shows that increasing the number of folds makes T_3 and T_4 more conservative. While Theorem 3.1 shows that T_ℓ

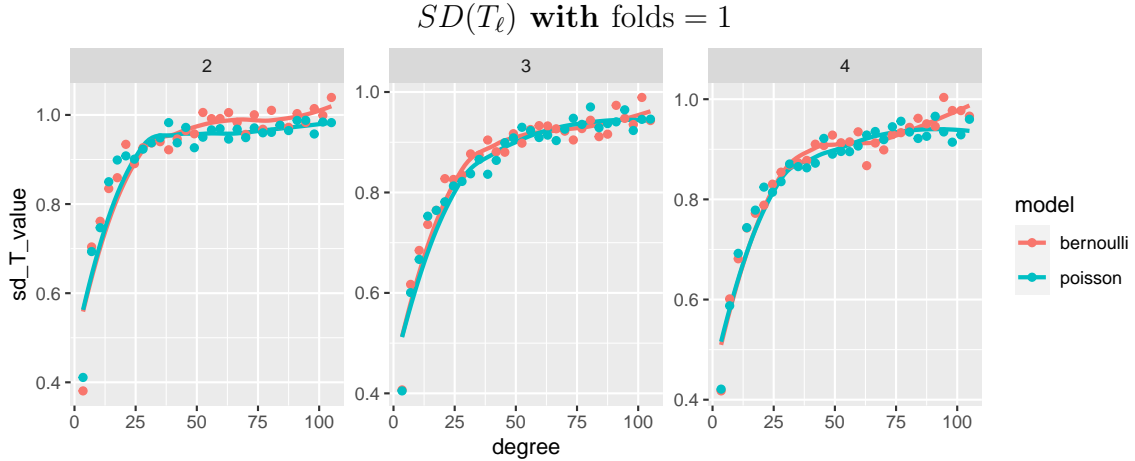


Figure S4: As discussed in Section S3, the localization of the eigenvectors on small degree graphs (on the left of each panel) makes $\tilde{\sigma}$ over estimate the standard error. This makes the standard deviation of the test statistics over the 1000 replicates smaller than 1.

is asymptotically normal with folds = 1, increasing the number of folds induces unknown dependence between the test statistics. Figure S5 suggests that even with 10 folds, the right tail of the distribution of T_3 and T_4 are well approximated by the normal distribution; this is because the bumpy line that gives $\hat{\alpha}$ is close to the points. The tests are conservative because their expectation is not zero and their variance is not one.

Figure S6 shows that increasing the number of folds dramatically reduces the variation in T_2, T_3, T_4 . This makes T_2 more powerful and T_3, T_4 more conservative.

S4 Additional information on the comparison of techniques

In Figure 4, we evaluated the accuracy of each method when requiring the exact recovery of k . In order to illustrate how each method either under-estimates or over-estimates k , Figure S7 displays the results in Figure 4 by the relative error for each estimate \hat{k} , which is defined as

$$\text{relative error} = \frac{\hat{k} - k^*}{k^*},$$

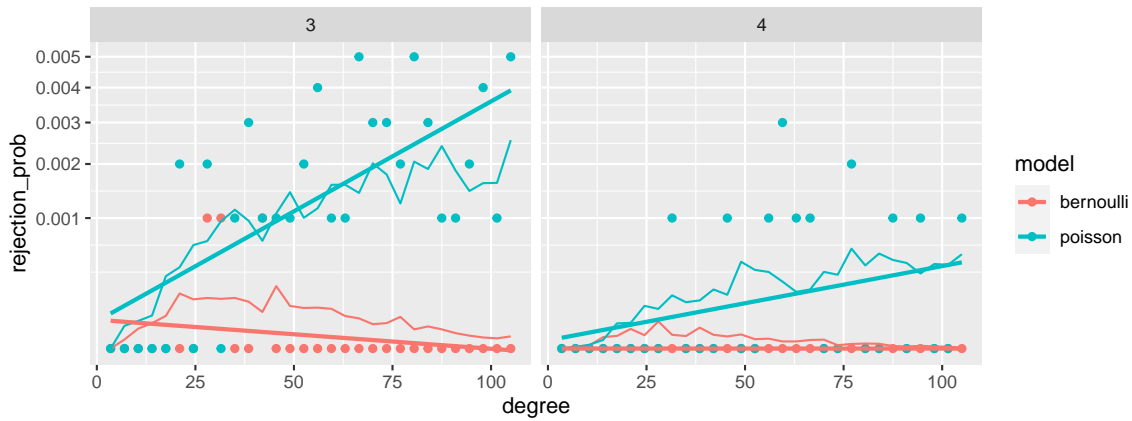


Figure S5: This is a repeat of Figure S1, but with folds = 10 instead of 1. The vertical axis gives estimates of the rejection probability for T_3 (left) and T_4 (right). Each dot give the proportion of 1000 simulations for which the test statistic exceeds 1.65. The bumpy line interpolates the values $\hat{\alpha}$, defined in Equation (S24). Because there are so few rejections, particularly for T_4 , it is difficult to see whether the bumpy line is close to the points. The straight line is the ordinary least squares fit to the points. It roughly aligns with the bumpy line. This suggests that the right tails of the distributions for T_3 and T_4 are approximately normally distributed.

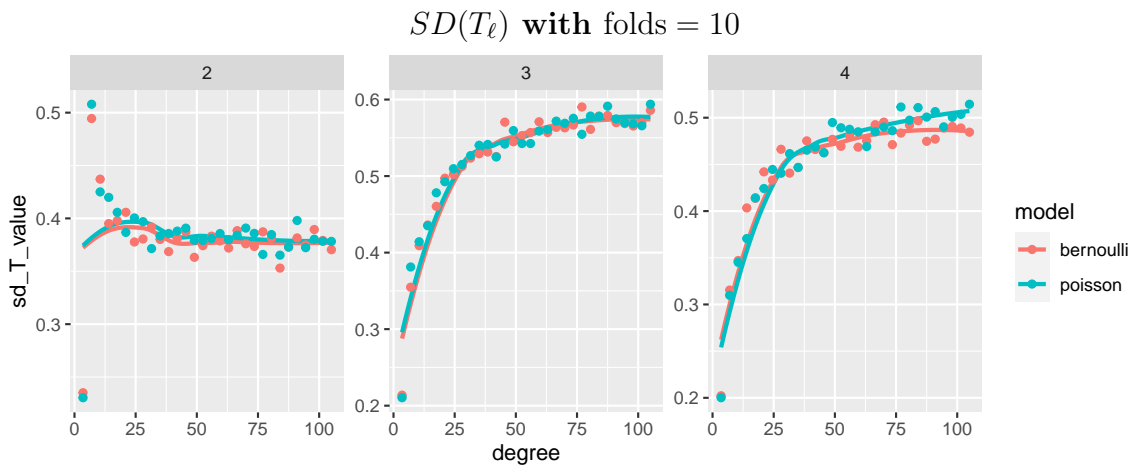


Figure S6: This is a repeat of Figure S4, but with folds = 10 instead of 1. The vertical axis gives the standard deviation of the test statistics T_2, T_3, T_4 over the 1000 replicates. Notice that they are all significantly less than one. This explains why the rejection probabilities in Figure S5 are significantly lower than .05.

where $k^* = 10$ is the true k . From the simulation results, we observed that most methods under-estimate k when the average degree of the graph is smaller (i.e., sparser), except for StGoF which over-estimates it. In addition, from the standard deviation of the relative error, we observe that EigCV provides a more accurate and less variable estimation of k as the graph sparsity varies.

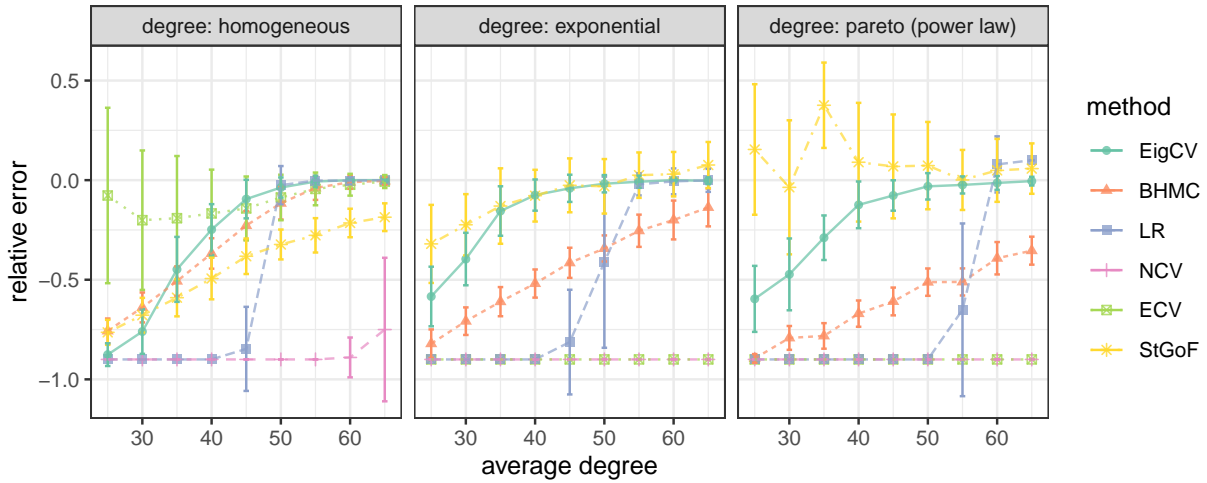


Figure S7: Comparison of relative error for different graph dimensionality estimators under the DCSBM. The panel strips on the top indicate the node degree distribution used. Within each panel, each colored line depicts the relative error of each estimation method as the average node degree increases. Each point on the lines are averaged across 100 repeated experiments. For each point, an error bar indicates the sample standard deviation of relative errors.

In Section 5.2, we removed the 14 small departments that consist of less than 10 members. Among these, two departments have only one members, and eight departments have less than five members. Table S1 compares six methods using this email network without filtering. We observed similarly that EigCV provided a closer estimate of k than other methods.

Table S1: Comparison of graph dimensionality estimates using the email network among members in a large European research institution. Each members belongs to one of 42 departments.

Method	Estimate (mean)	Runtime (second)
EigCV	30.56	0.81
BHMC	14.00	0.04
LR	13.00	128.17
NCV	6.96	271.15
ECV	20.08	60.13
StGoF	> 50	544.66

References

- Karim M. Abadir, Walter Distaso, and Filip Zikes. Design-free estimation of variance matrices. *Journal of Econometrics*, 181(2):165–180, August 2014. ISSN 0304-4076. doi: 10.1016/j.jeconom.2014.03.010. URL <https://www.sciencedirect.com/science/article/pii/S0304407614000591>.
- E. Abbe, A. S. Bandeira, and G. Hall. Exact Recovery in the Stochastic Block Model. *IEEE Transactions on Information Theory*, 62(1):471–487, January 2016. ISSN 1557-9654. doi: 10.1109/TIT.2015.2490670. Conference Name: IEEE Transactions on Information Theory.
- Emmanuel Abbe. Community Detection and Stochastic Block Models. *Foundations and Trends® in Communications and Information Theory*, 14(1-2):1–162, June 2018. ISSN 1567-2190, 1567-2328. doi: 10.1561/0100000067. URL <http://www.nowpublishers.com/article/Details/CIT-067>. Publisher: Now Publishers, Inc.
- Emmanuel Abbe and Colin Sandon. Community detection in general stochastic block models: fundamental limits and efficient recovery algorithms. *arXiv:1503.00609 [cs, math]*, April 2015. URL <http://arxiv.org/abs/1503.00609>. arXiv: 1503.00609.
- Emmanuel Abbe, Jianqing Fan, Kaizheng Wang, Yiqiao Zhong, et al. Entrywise eigenvector analysis of random matrices with low expected rank. *Annals of Statistics*, 48(3):1452–1474, 2020.
- Thomas D. Ahle. Sharp and Simple Bounds for the raw Moments of the Binomial and Poisson Distributions. *arXiv:2103.17027 [math, stat]*, April 2021. URL <http://arxiv.org/abs/2103.17027>. arXiv: 2103.17027.
- Edoardo Maria Airoldi, David M Blei, Stephen E Fienberg, and Eric P Xing. Mixed membership stochastic blockmodels. *Journal of machine learning research*, 2008.
- Oskari H. Ajanki, László Erdős, and Torben Krüger. Universality for general Wigner-type matrices. *Probability Theory and Related Fields*, 169(3):667–727, December 2017. ISSN 1432-2064. doi: 10.1007/s00440-016-0740-2. URL <https://doi.org/10.1007/s00440-016-0740-2>.
- David J Aldous. Exchangeability and related topics. In *École d’Été de Probabilités de Saint-Flour XIII—1983*, pages 1–198. Springer, 1985.
- Bloemendal Alex, László Erdős, Antti Knowles, Horng-Tzer Yau, and Jun Yin. Isotropic local laws for sample covariance and generalized Wigner matrices. *Electronic Journal of Probability*, 19, 2014. ISSN 1083-6489. doi: 10.1214/EJP.v19-3054. URL <http://projecteuclid.org/euclid.ejp/1465065675>. Publisher: The Institute of Mathematical Statistics and the Bernoulli Society.
- Waleed Ammar, Dirk Groeneveld, Chandra Bhagavatula, Iz Beltagy, Miles Crawford, Doug Downey, Jason Dunkelberger, Ahmed Elgohary, Sergey Feldman, Vu Ha, et al. Construction of the literature graph in semantic scholar. *arXiv preprint arXiv:1805.02262*, 2018.
- Ethan Ancell, Daniela Witten, and Daniel Kessler. Post-selection inference with a single realization of a network. *arXiv preprint arXiv:2508.11843*, 2025.
- Sylvain Arlot and Alain Celisse. A survey of cross-validation procedures for model selection. *Statistics Surveys*, 4(none):40–79, January 2010. ISSN 1935-7516. doi: 10.1214/09-SS054. URL <http://projecteuclid.org/journals/statistics-surveys/volume-4/issue-none/A-survey-of-cross-validation-procedures-for-model-selection/10.1214/09-SS054.full>. Publisher: Amer. Statist. Assoc., the Bernoulli Soc., the Inst. Math. Statist., and the Statist. Soc. Canada.

- Avanti Athreya, Vince Lyzinski, David J Marchette, Carey E Priebe, Daniel L Sussman, and Minh Tang. A central limit theorem for scaled eigenvectors of random dot product graphs. *arXiv preprint arXiv:1305.7388*, 2013.
- Tavor Z Baharav, David Tse, and Julia Salzman. Oasis: An interpretable, finite-sample valid alternative to pearson’s χ^2 for scientific discovery. *Proceedings of the National Academy of Sciences*, 121(15): e2304671121, 2024.
- Douglas Bates and Martin Maechler. *Matrix: Sparse and Dense Matrix Classes and Methods*, 2021. URL <https://CRAN.R-project.org/package=Matrix>. R package version 1.3-3.
- Florent Benaych-Georges, Charles Bordenave, and Antti Knowles. Largest eigenvalues of sparse inhomogeneous Erdős–Rényi graphs. *Annals of Probability*, 47(3):1653–1676, May 2019. ISSN 0091-1798, 2168-894X. doi: 10.1214/18-AOP1293. URL <http://projecteuclid.org/euclid.aop/1556784029>. Publisher: Institute of Mathematical Statistics.
- Florent Benaych-Georges, Charles Bordenave, and Antti Knowles. Spectral radii of sparse random matrices. *Annales de l’Institut Henri Poincaré, Probabilités et Statistiques*, 56(3):2141–2161, August 2020. ISSN 0246-0203. doi: 10.1214/19-AIHP1033. URL <http://projecteuclid.org/euclid.aihp/1593137322>. Publisher: Institut Henri Poincaré.
- Yoav Benjamini and Yosef Hochberg. Controlling the false discovery rate: a practical and powerful approach to multiple testing. *Journal of the Royal statistical society: series B (Methodological)*, 57(1):289–300, 1995.
- Sharmodeep Bhattacharyya and Peter J. Bickel. Subsampling bootstrap of count features of networks. *Annals of Statistics*, 43(6):2384–2411, December 2015. ISSN 0090-5364, 2168-8966. doi: 10.1214/15-AOS1338. URL <http://projecteuclid.org/euclid.aos/1444222079>. Publisher: Institute of Mathematical Statistics.
- Peter J. Bickel and Purnamrita Sarker. Hypothesis testing for automated community detection in networks. *Journal of the Royal Statistical Society. Series B (Statistical Methodology)*, 78(1):253–273, 2016. ISSN 1369-7412. URL <http://www.jstor.org/stable/24775336>. Publisher: [Royal Statistical Society, Wiley].
- C. Bordenave, M. Lelarge, and L. Massoulié. Non-backtracking Spectrum of Random Graphs: Community Detection and Non-regular Ramanujan Graphs. In *2015 IEEE 56th Annual Symposium on Foundations of Computer Science*, pages 1347–1357, October 2015. doi: 10.1109/FOCS.2015.86. ISSN: 0272-5428.
- S. Boucheron, G. Lugosi, and P. Massart. *Concentration Inequalities: A Nonasymptotic Theory of Independence*. OUP Oxford, 2013. ISBN 978-0-19-953525-5. URL <https://books.google.com/books?id=koNqWR1uhPOC>.
- Diana Cai, Trevor Campbell, and Tamara Broderick. Edge-exchangeable graphs and sparsity. In *Proceedings of the 30th International Conference on Neural Information Processing Systems*, pages 4249–4257, 2016.
- Emmanuel J Candès and Benjamin Recht. Exact matrix completion via convex optimization. *Foundations of Computational mathematics*, 9(6):717, 2009.
- Arijit Chakrabarty, Sukrit Chakraborty, and Rajat Subhra Hazra. Eigenvalues Outside the Bulk of Inhomogeneous Erdős–Rényi Random Graphs. *Journal of Statistical Physics*, 181(5):1746–1780, December 2020. ISSN 1572-9613. doi: 10.1007/s10955-020-02644-7. URL <https://doi.org/10.1007/s10955-020-02644-7>.

- Sourav Chatterjee. Matrix estimation by Universal Singular Value Thresholding. *The Annals of Statistics*, 43(1):177–214, February 2015. ISSN 0090-5364, 2168-8966. doi: 10.1214/14-AOS1272. URL <http://projecteuclid.org/journals/annals-of-statistics/volume-43/issue-1/Matrix-estimation-by-Universal-Singular-Value-Thresholding/10.1214/14-AOS1272.full>. Publisher: Institute of Mathematical Statistics.
- Fan Chen, Sebastien Roch, Karl Rohe, and Shuqi Yu. Estimating graph dimension with cross-validated eigenvalues. *arXiv preprint arXiv:2108.03336*, 2021.
- Kehui Chen and Jing Lei. Network Cross-Validation for Determining the Number of Communities in Network Data. *Journal of the American Statistical Association*, 113(521):241–251, January 2018. ISSN 0162-1459. doi: 10.1080/01621459.2016.1246365. URL <https://doi.org/10.1080/01621459.2016.1246365>. Publisher: Taylor & Francis eprint: <https://doi.org/10.1080/01621459.2016.1246365>.
- Harry Crane and Walter Dempsey. Edge exchangeable models for interaction networks. *Journal of the American Statistical Association*, 113(523):1311–1326, 2018.
- Ioana Dumitriu and Yizhe Zhu. Sparse general Wigner-type matrices: Local law and eigenvector delocalization. *Journal of Mathematical Physics*, 60(2):023301, February 2019. ISSN 0022-2488. doi: 10.1063/1.5053613. URL <https://aip-scitation-org.ezproxy.library.wisc.edu/doi/full/10.1063/1.5053613>. Publisher: American Institute of Physics.
- Rick Durrett. *Probability: Theory and Examples*. Cambridge Series in Statistical and Probabilistic Mathematics. Cambridge University Press, 5 edition, 2019. doi: 10.1017/9781108591034.
- László Erdős, Antti Knowles, Horng-Tzer Yau, and Jun Yin. Spectral Statistics of Erdős-Rényi Graphs II: Eigenvalue Spacing and the Extreme Eigenvalues. *Communications in Mathematical Physics*, 314(3): 587–640, September 2012. ISSN 1432-0916. doi: 10.1007/s00220-012-1527-7. URL <https://doi.org/10.1007/s00220-012-1527-7>.
- László Erdős, Antti Knowles, Horng-Tzer Yau, and Jun Yin. The local semicircle law for a general class of random matrices. *Electronic Journal of Probability*, 18, 2013. ISSN 1083-6489. doi: 10.1214/EJP.v18-2473. URL <http://projecteuclid.org/euclid.ejp/1465064284>. Publisher: The Institute of Mathematical Statistics and the Bernoulli Society.
- Cheryl Flynn, Patrick Perry, et al. Profile likelihood biclustering. *Electronic Journal of Statistics*, 14(1): 731–768, 2020.
- Alden Green and Cosma Rohilla Shalizi. Bootstrapping Exchangeable Random Graphs. *arXiv:1711.00813 [stat]*, November 2017. URL <http://arxiv.org/abs/1711.00813>. arXiv: 1711.00813.
- Peter D Hoff, Adrian E Raftery, and Mark S Handcock. Latent space approaches to social network analysis. *Journal of the American Statistical Association*, 97(460):1090–1098, 2002.
- DN Hoover. Tail fields of partially exchangeable arrays. *Journal of Multivariate Analysis*, 31(1):160–163, 1989.
- Jong Yun Hwang, Ji Oon Lee, and Wooseok Yang. Local law and Tracy–Widom limit for sparse stochastic block models. *Bernoulli*, 26(3):2400–2435, August 2020. ISSN 1350-7265. doi: 10.3150/20-BEJ1201. URL <http://projecteuclid.org/euclid.bj/1587974546>. Publisher: Bernoulli Society for Mathematical Statistics and Probability.

- Abigail Z Jacobs and Aaron Clauset. A unified view of generative models for networks: models, methods, opportunities, and challenges. *arXiv preprint arXiv:1411.4070*, 2014.
- Jiashun Jin, Zheng Tracy Ke, Shengming Luo, and Minzhe Wang. Estimating the number of communities by Stepwise Goodness-of-fit. *arXiv:2009.09177 [math, stat]*, September 2020. URL <http://arxiv.org/abs/2009.09177>. arXiv: 2009.09177.
- Antony Joseph and Bin Yu. Impact of regularization on spectral clustering. *Annals of Statistics*, 44(4):1765–1791, August 2016. ISSN 0090-5364, 2168-8966. doi: 10.1214/16-AOS1447. URL <http://projecteuclid.org/euclid.aos/1467894715>. Publisher: Institute of Mathematical Statistics.
- Brian Karrer and M. E. J. Newman. Stochastic blockmodels and community structure in networks. *Physical Review E*, 83(1):016107, January 2011. doi: 10.1103/PhysRevE.83.016107. URL <https://link.aps.org/doi/10.1103/PhysRevE.83.016107>. Publisher: American Physical Society.
- Florent Krzakala, Cristopher Moore, Elchanan Mossel, Joe Neeman, Allan Sly, Lenka Zdeborová, and Pan Zhang. Spectral redemption in clustering sparse networks. *Proceedings of the National Academy of Sciences*, 110(52):20935–20940, December 2013. ISSN 0027-8424, 1091-6490. doi: 10.1073/pnas.1312486110. URL <http://www.pnas.org/content/110/52/20935>. Publisher: National Academy of Sciences Section: Physical Sciences.
- Clifford Lam. Nonparametric eigenvalue-regularized precision or covariance matrix estimator. *The Annals of Statistics*, 44(3):928–953, June 2016. ISSN 0090-5364, 2168-8966. doi: 10.1214/15-AOS1393. URL <http://projecteuclid.org/journals/annals-of-statistics/volume-44/issue-3/Nonparametric-eigenvalue-regularized-precision-or-covariance-matrix-estimator/10.1214/15-AOS1393.full>. Publisher: Institute of Mathematical Statistics.
- Can M. Le and Elizaveta Levina. Estimating the number of communities in networks by spectral methods. *arXiv:1507.00827 [cs, math, stat]*, November 2019. URL <http://arxiv.org/abs/1507.00827>. arXiv: 1507.00827.
- Can M. Le, Elizaveta Levina, and Roman Vershynin. Concentration and regularization of random graphs. *Random Structures & Algorithms*, 51(3):538–561, 2017. ISSN 1098-2418. doi: 10.1002/rsa.20713. URL <https://onlinelibrary.wiley.com/doi/abs/10.1002/rsa.20713>. eprint: <https://onlinelibrary.wiley.com/doi/pdf/10.1002/rsa.20713>.
- Jing Lei. A goodness-of-fit test for stochastic block models. *Annals of Statistics*, 44(1):401–424, February 2016. ISSN 0090-5364, 2168-8966. doi: 10.1214/15-AOS1370. URL <http://projecteuclid.org/euclid.aos/1452004791>. Publisher: Institute of Mathematical Statistics.
- Jure Leskovec, Jon Kleinberg, and Christos Faloutsos. Graph evolution: Densification and shrinking diameters. *ACM transactions on Knowledge Discovery from Data (TKDD)*, 1(1):2–es, 2007.
- Keith Levin and Elizaveta Levina. Bootstrapping Networks with Latent Space Structure. *arXiv:1907.10821 [math, stat]*, July 2019. URL <http://arxiv.org/abs/1907.10821>. arXiv: 1907.10821.
- Tianxi Li, Elizaveta Levina, and Ji Zhu. Network cross-validation by edge sampling. *Biometrika*, 107(2): 257–276, June 2020. ISSN 0006-3444. doi: 10.1093/biomet/asaa006. URL <https://doi.org/10.1093/biomet/asaa006>.
- Qiaohui Lin, Robert Lunde, and Purnamrita Sarkar. Higher-Order Correct Multiplier Bootstraps for Count Functionals of Networks. *arXiv:2009.06170 [math, stat]*, September 2020a. URL <http://arxiv.org/abs/2009.06170>. arXiv: 2009.06170.

- Qiaohui Lin, Robert Lunde, and Purnamrita Sarkar. On the Theoretical Properties of the Network Jack-knife. In *International Conference on Machine Learning*, pages 6105–6115. PMLR, November 2020b. URL <http://proceedings.mlr.press/v119/lin20c.html>. ISSN: 2640-3498.
- Yan Liu, Zhiqiang Hou, Zhigang Yao, Zhidong Bai, Jiang Hu, and Shurong Zheng. Community Detection Based on the L_∞ convergence of eigenvectors in DCBM. *arXiv:1906.06713 [math, stat]*, June 2019. URL <http://arxiv.org/abs/1906.06713>. arXiv: 1906.06713.
- László Lovász. *Large networks and graph limits*, volume 60. American Mathematical Soc., 2012.
- Robert Lunde and Purnamrita Sarkar. Subsampling Sparse Graphons Under Minimal Assumptions. *arXiv:1907.12528 [math, stat]*, August 2019. URL <http://arxiv.org/abs/1907.12528>. arXiv: 1907.12528.
- Shujie Ma, Liangjun Su, and Yichong Zhang. Determining the Number of Communities in Degree-corrected Stochastic Block Models. *arXiv:1809.01028 [stat]*, July 2019. URL <http://arxiv.org/abs/1809.01028>. arXiv: 1809.01028.
- Elchanan Mossel, Joe Neeman, and Allan Sly. Reconstruction and estimation in the planted partition model. *Probability Theory and Related Fields*, 162(3):431–461, 2015.
- Zacharie Naulet, Daniel M. Roy, Ekansh Sharma, and Victor Veitch. Bootstrap estimators for the tail-index and for the count statistics of graphex processes. *Electronic Journal of Statistics*, 15(1):282–325, 2021. ISSN 1935-7524. doi: 10.1214/20-EJS1789. URL <http://projecteuclid.org/euclid.ejs/1609902191>. Publisher: The Institute of Mathematical Statistics and the Bernoulli Society.
- Anna Neufeld, Ameer Dharamshi, Lucy L Gao, and Daniela Witten. Data thinning for convolution-closed distributions. *Journal of Machine Learning Research*, 25(57):1–35, 2024a.
- Anna Neufeld, Lucy L Gao, Joshua Popp, Alexis Battle, and Daniela Witten. Inference after latent variable estimation for single-cell rna sequencing data. *Biostatistics*, 25(1):270–287, 2024b.
- Richard R. Picard and R. Dennis Cook. Cross-Validation of Regression Models. *Journal of the American Statistical Association*, 79:575–583, 1984. ISSN 0162-1459. doi: 10.2307/2288403. URL <http://www.jstor.org/stable/2288403>. Publisher: [American Statistical Association, Taylor & Francis, Ltd.].
- Tai Qin and Karl Rohe. Regularized spectral clustering under the degree-corrected stochastic blockmodel. In *Proceedings of the 26th International Conference on Neural Information Processing Systems-Volume 2*, pages 3120–3128, 2013.
- Yixuan Qiu and Jiali Mei. *RSpectra: Solvers for Large-Scale Eigenvalue and SVD Problems*, 2019. URL <https://CRAN.R-project.org/package=RSpectra>. R package version 0.16-0.
- Karl Rohe and Muzhe Zeng. Vintage factor analysis with varimax performs statistical inference. *arXiv preprint arXiv:2004.05387*, 2020.
- Karl Rohe, Sourav Chatterjee, and Bin Yu. Spectral clustering and the high-dimensional stochastic blockmodel. *Annals of Statistics*, 39(4):1878–1915, August 2011. ISSN 0090-5364, 2168-8966. doi: 10.1214/11-AOS887. URL <http://projecteuclid.org/euclid.aos/1314190618>. Publisher: Institute of Mathematical Statistics.
- Karl Rohe, Jun Tao, Xintian Han, and Norbert Binkiewicz. A note on quickly sampling a sparse matrix with low rank expectation. *Journal of Machine Learning Research*, 19(77):1–13, 2018. URL <http://jmlr.org/papers/v19/17-128.html>.

- Tom AB Snijders and Stephen P Borgatti. Non-parametric standard errors and tests for network statistics. *Connections*, 22(2):161–170, 1999.
- Alexander Soshnikov. Universality at the Edge of the Spectrum in Wigner Random Matrices. *Communications in Mathematical Physics*, 207(3):697–733, November 1999. ISSN 1432-0916. doi: 10.1007/s002200050743. URL <https://doi.org/10.1007/s002200050743>.
- Liangjun Su, Wuyi Wang, and Yichong Zhang. Strong Consistency of Spectral Clustering for Stochastic Block Models. *arXiv:1710.06191 [stat]*, May 2019. URL <http://arxiv.org/abs/1710.06191>. arXiv: 1710.06191.
- Mary E. Thompson, Lilia L. Ramirez Ramirez, Vyacheslav Lyubchich, and Yulia R. Gel. Using the bootstrap for statistical inference on random graphs. *Canadian Journal of Statistics*, 44(1):3–24, 2016. ISSN 1708-945X. doi: <https://doi.org/10.1002/cjs.11271>. URL <http://onlinelibrary.wiley.com/doi/abs/10.1002/cjs.11271>. eprint: <https://onlinelibrary.wiley.com/doi/pdf/10.1002/cjs.11271>.
- Craig A. Tracy and Harold Widom. Level-spacing distributions and the Airy kernel. *Communications in Mathematical Physics*, 159(1):151–174, January 1994. ISSN 1432-0916. doi: 10.1007/BF02100489. URL <https://doi.org/10.1007/BF02100489>.
- Joel A Tropp. User-friendly tail bounds for sums of random matrices. *Foundations of computational mathematics*, 12(4):389–434, 2012.
- Y. X. Rachel Wang and Peter J. Bickel. Likelihood-based model selection for stochastic block models. *Annals of Statistics*, 45(2):500–528, April 2017. ISSN 0090-5364, 2168-8966. doi: 10.1214/16-AOS1457. URL <http://projecteuclid.org/euclid.aos/1494921948>. Publisher: Institute of Mathematical Statistics.
- Yi Yu, Tengyao Wang, and Richard J Samworth. A useful variant of the Davis–Kahan theorem for statisticians. *Biometrika*, 102(2):315–323, 2015.
- Yilin Zhang and Karl Rohe. Understanding regularized spectral clustering via graph conductance. In *Proceedings of the 32nd International Conference on Neural Information Processing Systems*, NIPS’18, page 10654–10663, Red Hook, NY, USA, 2018. Curran Associates Inc.
- Zhixin Zhou and Arash A. Amini. Optimal bipartite network clustering. *Journal of Machine Learning Research*, 21(40):1–68, 2020. URL <http://jmlr.org/papers/v21/19-299.html>.
- Mu Zhu and Ali Ghodsi. Automatic dimensionality selection from the scree plot via the use of profile likelihood. *Computational Statistics & Data Analysis*, 51(2):918–930, November 2006. ISSN 0167-9473. doi: 10.1016/j.csda.2005.09.010. URL <https://www.sciencedirect.com/science/article/pii/S0167947305002343>.